Journal of Medicinal Chemistry

pubs.acs.org/jmc Article

Discovering High Potent Hsp90 Inhibitors as Antinasopharyngeal Carcinoma Agents through Fragment Assembling Approach

Mengyang Xu, Chao Zhao, Biying Zhu, Liangyue Wang, Huihao Zhou, Daoguang Yan,* Qiong Gu,* and Jun Xu*

Cite This: *J. Med. Chem.* 2021, 64, 2010−2023 Read Online

ACCESS | Metrics & More | Article Recommendations | Supporting Information

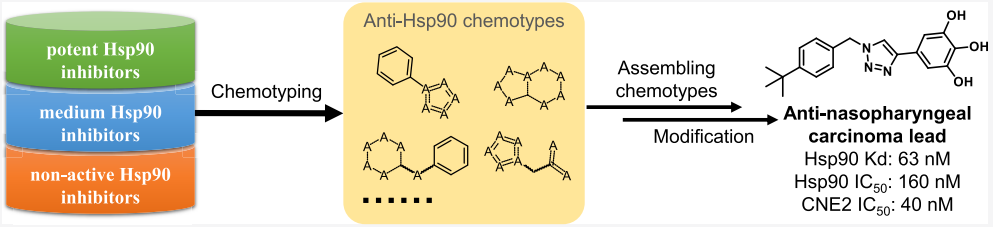

ABSTRACT: Hsp90 is a new promising target for cancer treatment. Many inhibitors have been discovered as therapeutic agents, and some have passed Phase I and II. However, no one is approved by FDA yet. Novel and druggable Hsp90 inhibitors are still demanding. Here, we report a new way to discover high potent Hsp90 inhibitors as antinasopharyngeal carcinoma agents through assembling fragments. With chemotyping analysis, we extract seven chemotypes from 3482 known Hsp90 inhibitors, screen 500 fragments that are compatible with the chemotypes, and confirm 15 anti-Hsp90 fragments. Click chemistry is employed to construct 172 molecules and synthesize 21 compounds among them. The best inhibitor 3d was further optimized and resulted in more potent 4f (IC_{50} = 0.16 μM). *In vitro* and *in vivo* experiments confirmed that 4f is a promising agent against nasopharyngeal carcinoma. This study may provide a strategy in discovering new ligands against targets without well-understood structures.

INTRODUCTION

Heat shock protein 90 (Hsp90, a molecular chaperone participating in the regulation of cell proliferation and apoptosis) is highly expressed in tumor cells. More than 200 oncogenic proteins are clients of Hsp90, such as HER2, EGFR, AKT, p53, BCR-ABL, and Raf.[1] Targeting Hsp90 is a new promising strategy for anticancer drug development.[2] Recently, Hsp90 was reported to play an important role in virus infection such as Dengue virus and Epstein−Barr virus,[3−8] and Hsp90 inhibitors were used to treat aging-related disease.[9,10]

Hsp90 consists of N-terminal domain for adenosine triphosphate (ATP) binding, middle domain for client protein binding, and C-terminal domain for dimerization. ATP binding causes Hsp90 conformational change, which activates Hsp90 chaperone function. Thus, many ATP-competitive inhibitors were developed to disrupt Hsp90 function for treating cancers. These inhibitors belong to three major classes: (1) geldanamycin analogues,[11] such as 17-DMAG,[12] 17-AAG,[13] and IPI-504;[14] (2) radicicol derivatives like NVP-AUY922,[15] STA-9090,[16] and AT13387;[17] and (3) purine-based Hsp90 inhibitors such as BIIB021.[18,19] Over 20 Hsp90 N-terminal inhibitors entered clinical trials; however, they were all discontinued due to toxicity. Therefore, novel druggable Hsp90 inhibitors are still demanding.

Fragment-based drug discovery (FBDD) has been employed for years with significant success.[20−25] FBDD starts with a smaller number of fragments[26] rather than screening a large number of druglike compounds. There can be $10^{60−200}$ possible druglike compounds, but only 10^7 possible fragments.[27] FBDD can significantly reduce chemical space for lead identification.[28] However, optimizing fragments to leads (F2L) is still a challenge for FBDD. Fragment growing, merging, and linking are common techniques for F2L. These techniques require well-understood fragment−receptor binding models, which have to be supported by structure biology experiments.[29] Moreover, F2L has to chemically combine fragments with the binding model restructions.[30]

To develop new approaches for combining fragments, we reported a strategy that discovered liver X receptor-β (LXRβ) agonists by connecting LXRβ privileged fragments that extracted from known LXRβ agonists.[31] Later on, we reported a promoted strategy called chemotype-based drug discovery (CBDD) and identified antiosteoporosis leads with the chemotyping analysis approach and their assembly rules.[32] These results indicate that compounds with same target or

Received: September 3, 2020
Published: February 5, 2021

https://dx.doi.org/10.1021/acs.jmedchem.0c01521
J. Med. Chem. 2021, 64, 2010−2023

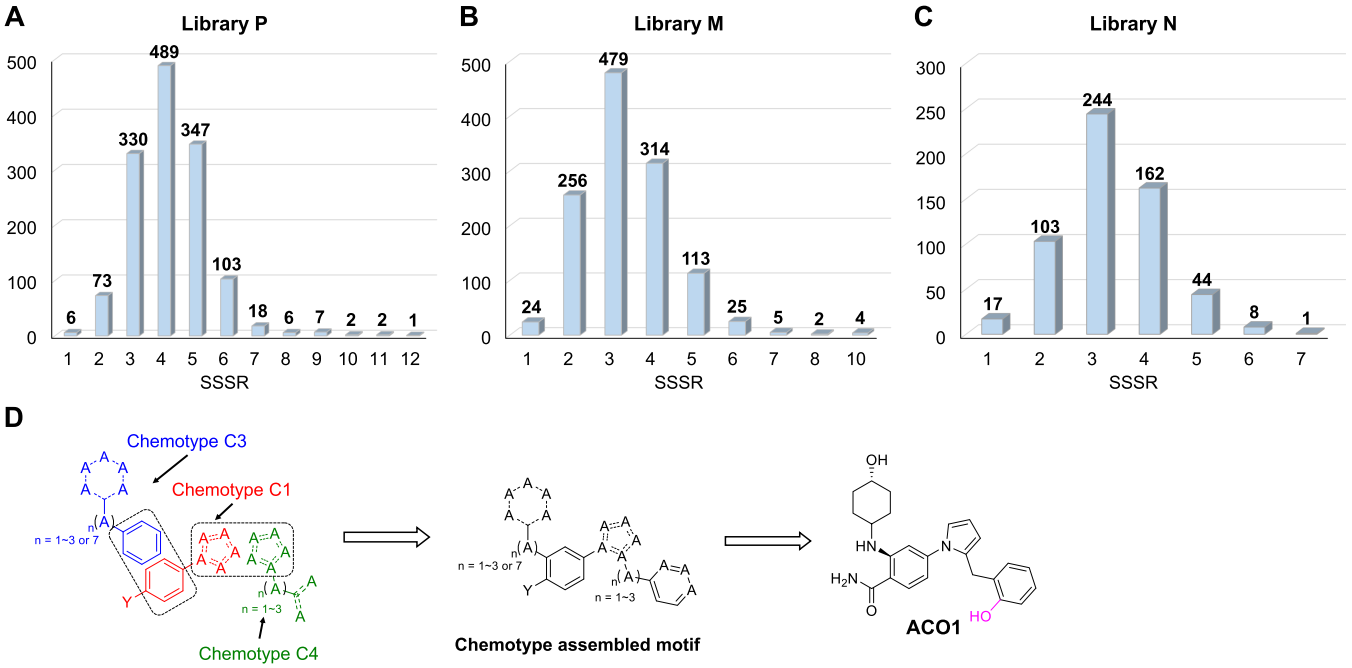

Figure 1. (A) SSSR of molecules in Library P. (B) The SSSR of molecules in Library M. (C) The SSSR of molecules in Library N. (D) The example of chemotypes assembly to known Hsp90 inhibitor ACO1. The pink color shows that the functional group does not include in chemotype-assembled motif. SSSR = smallest set of smallest rings.

function constructed with chemotypes through certain rules. This may help us to accelerate the F2L process and discovery novel Hsp90 inhibitors.

In this study, we report a second-generation CBDD method that utilizes both fragment-linking approach and the chemotyping analysis approach. And we apply this method in the discovery of novel Hsp90 inhibitors.

RESULTS

Chemotypes Derived from Known Anti-Hsp90 Agents. We started with 3482 known Hsp90 inhibitors derived from ChEMBL database. These inhibitors partitioned into potent library (library P, 1384 inhibitors with pChEMBL values greater than 6), moderate potent library (library M, 1233 inhibitors with pChEMBL values between 6 and 5), and nonactive library (library N, 865 inhibitors with pChEMBL values less than 5). The smallest set of smallest rings (SSSR) analyses indicated that inhibitors with three rings were most popular (Figure 1), and potent Hsp90 inhibitors had at least two rings. Therefore, we hypothesize that Hsp90 inhibitors can be generated by linking chemotypes that have same ring in each fragment.

Using a de novo substructure generation algorithm (DSGA), we derived 29 privileged fragments (PF) and 164 other fragments. Many privileged fragments of Hsp90 inhibitors have five- or six-membered rings. The privileged fragments were summarized into four motifs (**PF1−4**, Table 1). **PF1** and **PF4** exhibited much higher popularity in library P than libraries M and N. **PF2** and **PF3** showed that even frequency in all libraries.

The chemotypes and their popularities are listed in Table 1, which indicates that library P contains more chemotypes **C1** and **C2** than libraries M and N do. Thus, we hypothesize that compounds containing **C1** and **C2** can be more potent Hsp90 inhibitors. Chemotype **C3** is associated with mild Hsp90 inhibition, which is related to the compounds in libraries P and M. The popularities of chemotypes **C4−6** are evenly distributed in all three libraries. Chemotype **C7** is a rare chemotype. Thus, we hypothesize that linking chemotypes **C1** and **C4** can generate more potent Hsp90 inhibitors. A potent known Hsp90 inhibitor **ACO1** is assembled by **C1**, **C3**, and **C4** (Figure 1D). The chemotypes **C1** and **C3** link through merging six-membered aromatic rings, and then newly formed motif link with **C4** through overlapping the same five-membered aromatic ring. This indicated that Hsp90 inhibitor can be formed by linking anti-Hsp90 chemotypes.

Novel Hsp90 Inhibitors Design Based on Newly Discovered Active Anti-Hsp90 Fragments. A library containing 500 fragments were virtually screened based on the PFs and chemotypes via substructure retrieval, resulting in 328 fragments, which were then acquired and assayed with surface plasmon resonance (SPR)[33] experiments. Thus, we identified 28 hits (Figure 2A) that exhibited a response value higher than 30. The hits are all compatible with the privileged chemotypes of Hsp90 inhibitors. For instance, hits F01-04 belong to mono-ring PF1 and F14-16 belong to chemotype C1. These results imply that they all can be used to generate potential Hsp90 inhibitors.

Linking chemotypes **C1**, **C4**, and **C7** to form triazole derivatives can be efficiently executed with click chemistry syntheses. This requires converting out hits (fragments) to brominated or alkynyl products as starting materials for click chemistry reactions. Thus, the hits with multisubstituted fragments were simplified to mono-substituted fragments (precursors of brominated or alkynyl products) with the condition of commercial availability (Figure 2E). This resulted in seven bromides and two alkynes as the precursors, and two designed scaffolds for potential Hsp90 inhibitory molecules, as shown in Figure 2B. For negative control, we purposely assembled molecules that contained chemotypes that were not considered as Hsp90 inhibitory fragments (such as 2-

https://dx.doi.org/10.1021/acs.jmedchem.0c01521
J. Med. Chem. 2021, 64, 2010−2023

Table 1. Privileged Anti-Hsp90 Chemotypes and Their Frequency in Different Libraries[ae]

ID	Chemotype[a]	Frequency		
		Library P[b]	Library M[c]	Library N[d]
PF1[e]		70.88%	44.20%	40.23%
PF2		24.57%	25.71%	26.94%
PF3		39.74%	30.74%	36.99%
PF4		23.19%	13.79%	11.10%
C1		48.7%	15.6%	12.3%
C2		48.4%	18.5%	25.1%
C3		19.4%	14.3%	6.6%
C4		20.0%	18.6%	24.9%
C5		15.4%	11.8%	9.2%
C6		6.80%	16.1%	10.8%
C7		1.4%	0.0%	0.0%

[a]A = nonhydrogen atom, usually is C, O, N, and S; Q = nonhydrogen heteroatom; Y = any function group, such as C, N, O, S, $CONH_2$, CH_2OH, etc. Dashed lines = any bonds (single or double bond). Double dashed lines = aromatic bond. [b]Library P = potent library. [c]Library M = moderate potent library. [d]Library N = nonactive library. [e]PF = privileged fragments.

ethynylthiophene). Twenty-one compounds (Table 2) were synthesized with the scheme shown in Figure 2D.

Anti-Hsp90 and Nasopharyngeal Carcinoma Hit Discovered. We validated the inhibitory activities of the synthesized compounds with Hsp90α ATPase assay. Our results indicated that most compounds containing the Hsp90 binding chemotypes (see **3a**−**3n** in Table 2) exhibited Hsp90 inhibitory activities indeed. However, compounds (see **3o**−**3u** in Table 2) with other chemotypes (see Figure 2C) significantly lost activities (lower than 10% inhibition at 10 μM). Compounds **3d** and **3n** also showed potent binding affinity with Hsp90α and Hsp90β as well as their inhibition effects (Table 3). Furthermore, the cytotoxicities of **3d** and **3n** were tested on liver cancer, cervical carcinoma, and nasopharyngeal carcinoma (Table 3). Compound **3d** selectively inhibits nasopharyngeal carcinoma with an IC_{50} value of 3.98 μM. Compound **3d** provides a hit scaffold for further study.

Binding Model of Hit Compound 3d with Hsp90. Molecular dynamic[34] simulations indicate that **3d** binds to the ATP binding pocket of Hsp90α (Figure 3, PDB ID: 4W7T) through two hydrogen bonds with Thr184 (one of the hydrogen bonds is through a water bridge). Also, a water-mediated interaction net connects **3d**'s triazole ring to Phe138 and Asn51, which makes the *t*-butyl benzene ring be docked into a hydrophobic pocket formed with Ala111, Tyr139, Leu107, Phe22, Trp162, and Phe138. This compound does not interact with the key residue Asp93. To further enhance the activity of **3d**, the benzene ring needs to be modified to establish the binding between **3d** and Asp93 (Table 4). Compared to NVP-HSP990 and NVP-AUY992, compound **3d** occupied a different hydrophobic pocket by the *t*-butyl benzyl group (Figure 3B,C), and this is similar to TAS-116 (Figure 3D).

Anti-Hsp90 Lead Compound 4f Discovered. Hence, we synthesized seven **3d** derivatives (**4a**−**4f**) by introducing −OH or $-NH_2$ groups onto the scaffold of **3d**. These derivatives exhibited enhanced Hsp90α or Hsp90β inhibitory activities. Specifically, the compounds with *para*-hydroxyl benzene have significantly increased Hsp90 inhibitory activities. However, the $-NH_2$ group in ortho position suppresses the activity. The intermediate compound **5a** further revealed that *ortho*-NH_2 decreases the Hsp90 inhibition effect. As we hypothesize before, the hydroxy groups do increase the activity like **4f** 16-fold more potent than **5a**. Among them, compound **4f** showed 5-fold more potent Hsp90 inhibition effects than 17-AAG.

A molecular dynamics simulation indicates that more binding interactions were formed between 4f and Hsp90α (PDB ID: 4W7T) compared to compound **4a** (Figure 4). As expected, two hydroxy groups of **4f** provide two more hydrogen bonds with Asp93 and one more hydrogen bond with Thr184 compared to **3d**. Another hydroxy group forms a water-mediated hydrogen bond with Met98. The α-carbon of benzyl provides a hydrogen-bond network with Asn51, Gly135, and Phe138 through water. A p−π conjugation is formed between Leu107 and *tert*-butyl benzene ring. When Asp93 was mutated to Gly93, the binding affinity between **4f** and Hsp90α was decreased in 1600-fold (the table in Figure 4). The mutations at Leu71 and Thr184 also result in a significant decrease of Hsp90 binding affinity. These data proved that the binding model is reasonable.

Compound 4f Prevents Nasopharyngeal Carcinoma *in vivo* and *in vitro* through Inhibiting Hsp90. The activity of these newly synthesized compounds was tested on nasopharyngeal carcinoma (see the last column in Tables 4 and S3). Compound **4f** exhibited the most potent activity in a dose-dependent manner without cytotoxicity on normal cells (Figures 5A and S2, Table S3). Protein kinase B (PKB, *aka* AKT, an Hsp90 client protein) (Figures 5B and S3) was degraded through the induction of compound **4f** without changing Hsp90 expression. Thus, PI3K/AKT signaling pathway, which activates many cell survival-related proteins, is regulated. Consequently, **4f** causes the CNE2 cell apoptosis through PI3K/AKT signaling pathway. The degradation of protein B-cell lymphoma-extra large (Bcl-xL) indicates that compound **4f** may induce mitochondrial-mediated apoptosis in CNE2 cells. Another key protein HER2 related to cell death was also decreased at 500 nM. All of these data revealed that **4f** causes cell apoptosis through a multipathway, proteostasis disruption.

Figure 5C,D also demonstrates that **4f** cannot induce the CNE2 cell apoptosis after two different Hsp90 siRNAs were treated and **4f** cannot alter the amount of AKT and Bcl-xL after knockdown of the Hsp90 gene. These data proved that **4f** does induce the CNE2 cell apoptosis through Hsp90

https://dx.doi.org/10.1021/acs.jmedchem.0c01521
J. Med. Chem. 2021, 64, 2010−2023

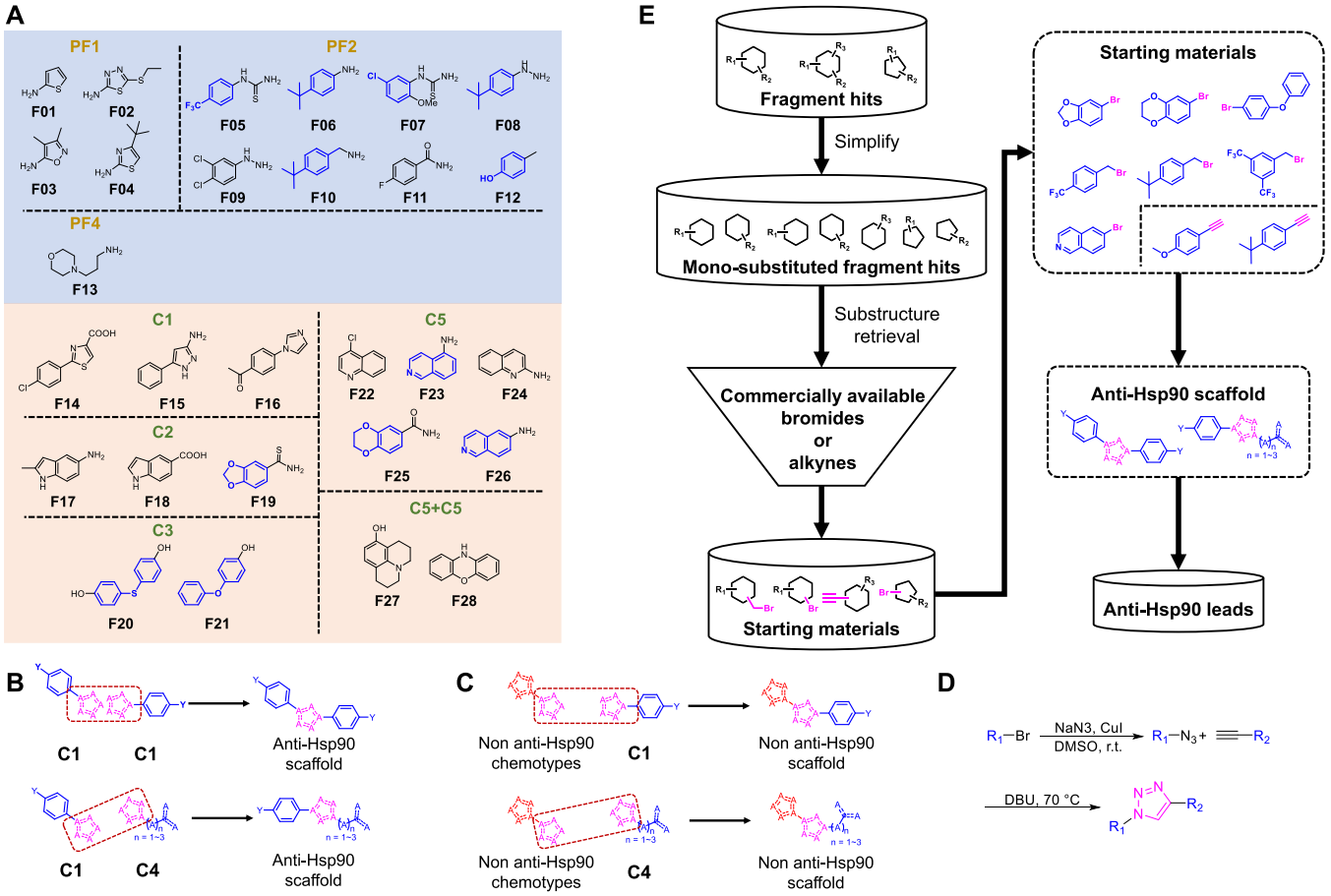

Figure 2. Designing Hsp90 inhibitors through assembling privileged chemotypes. (A) Thirty fragments for building potential Hsp90 inhibitors. 5Har = five-membered heteroaromatic ring; 6Ar = six-membered aromatic ring; 6r = six-membered aliphatic ring. (B) Chemotypes assembling to form potential anti-Hsp90 scaffolds. (C) Chemotype **C1** or **C4** assembles with a non-anti-Hsp90 chemotype to form potential non-anti-Hsp90 scaffolds. (D) Click chemistry synthetical scheme for assembling potential Hsp90 inhibitors from privileged fragments (chemotypes). (E) Commercially available starting materials from active fragments.

inhibition. Another rescue assay further confirmed that **4f** cause CNE2 apoptosis through Hsp90 inhibition. As shown in Figure 5E, the overexpression of Hsp90 can rescue the cell compared to the mock group (not Hsp90 overexpression) after **4f** treatment. However, without treating **4f**, the cell apoptosis is quite similar between the mock group and the Hsp90 overexpression group. The amounts of related proteins like AKT and BCL2 were also increased by Hsp90 overexpression.

As shown in Figure 6A,B, *in vivo* studies demonstrated that the tumor sizes were shrunken after 32-day treatment with **4f**. Figure 6C indicates that **4f** can inhibit the nasopharyngeal tumor growth in a time-dependent manner. Finally, a pharmacokinetic (PK) study was applied to test the druggable property. As shown in Figure 6D, $t_{1/2}$ of **4f** is 1.10 h and the bioavailability (F value) is 12%.

DISCUSSION

Here, we reported a novel strategy of hit fragments discovering and assembling. The most potent compound **4f** was confirmed as an Hsp90 inhibitor to treat nasopharyngeal carcinoma by *in vitro* and *in vivo* studies. First, we discovered PFs and chemotypes from known Hsp90. These PFs and chemotypes were then applied for hit fragments discovery. Here, seven main fragments were found, four of which were considered as privileged fragments, two were considered as normal fragments (NFs, Table S1), and the last one is considered as a bad fragment (BF, Table S1). Like PFs, the NFs also exhibit higher frequency in library P than the other two libraries (Table S1). However, their frequency in library P is much lower than PFs (NF1 is 4.19% and NF2 is 2.82%). Different from PFs and NFs, the frequency of BF1 in nonactive library is higher than the other two libraries (4.28% in library N vs 3.68% in library P and 2.11% in library M). Therefore, we consider it as BF because it may decrease activities. The fragments that contain BF1 were also filtered before SPR screening. According to the PFs and BF, 328 hit fragments were extracted from 500 and then confirmed by SPR. The chemotypes are defined as two fragments from PFs and BFs assembled through the linker between them. The linkers are discovered according to our previous study.[32] In this study, PFs and chemotypes are applied for screening fragments to discover potential anti-Hsp90 hit fragments. Since the PFs and chemotypes are extracted from known compounds, they can be employed to build specific fragment databases for given targets in future. These databases may provide a higher success rate of hit fragment identification.

The process of optimizing the hit fragments to leads is usually considered as the bottleneck of FBDD. In most cases, it is difficult to understand fragment−protein interactions (reasonable binding model of fragment−protein), which plays a key role in the F2L process. Theoretically, chemotypes

https://dx.doi.org/10.1021/acs.jmedchem.0c01521
J. Med. Chem. 2021, 64, 2010−2023

Table 2. Structures of 15 Newly Designed Compounds and Their Hsp90 Inhibitory Activities

Compds	Structures	%Inhibition[a]	Compds	Structures	%Inhibition[a]
3a	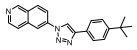	13.7	**3l**	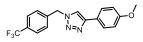	29.3
3b	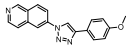	8.2	**3m**	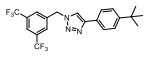	24.6
3c	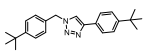	20.1	**3n**	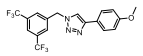	46.4
3d	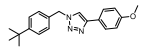	58.9	**3o**	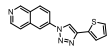	2.7
3e	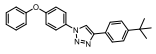	16.4	**3p**	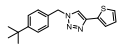	5.5
3f	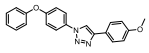	21.9	**3q**	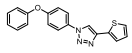	15.5
3g	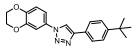	16.4	**3r**	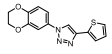	9.6
3h	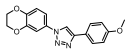	19.9	**3s**	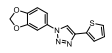	2.8
3i	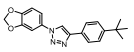	18.3	**3t**	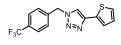	10.4
3j	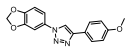	8.2	**3u**	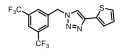	8.9
3k	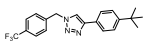	14.2	**17-AAG**		80.1

[a]The percent of Hsp90α ATPase activity inhibition at the 10 μM of testing compounds.

Table 3. Chemotype-Constructed Substructures and Their Frequency

bioassays	3d	3n	17-AAG
Hsp90α K_d (μM)[a]	4.8 ± 0.5	3.1 ± 0.4	0.9 ± 0.1
Hsp90β K_d (μM)[a]	4.8 ± 1.0	7.0 ± 1.5	0.9 ± 0.2
Hsp90α IC_{50} (μM)[b]	5.6 ± 0.3	6.2 ± 1.4	0.9 ± 0.3
Hsp90β IC_{50} (μM)[b]	5.6 ± 1.1	9.8 ± 1.5	0.8 ± 0.1
HepG2[c] IC_{50} (μM)	>50	18.1 ± 1.9	8.0 ± 2.0
Hela[d] IC_{50} (μM)	>50	22.4 ± 3.3	19.4 ± 3.2
CNE2[e] IC_{50} (μM)	4.0 ± 0.5	14.1 ± 2.1	3.0 ± 0.6

[a]K_d is tested by SPR. [b]IC_{50} indicates ATPase inhibition effects. [c]HepG2 indicates liver cancer. [d]Hela indicates cervical carcinoma. [e]CNE2 denotes nasopharyngeal carcinoma.

can assemble with each other to grow up through same ring overlapping (including homo- and hetero-assembling, Figure 1D). This strategy provides a possibility for optimizing fragments when the fragment−protein binding model is difficult to obtain. Our study proved that chemotype assembly can be used for the F2L process without understanding fragment−protein interactions. The novelty of leads discovered by this method is warranted. The combination of different chemotypes provides various novel scaffolds. For example, only two chemotypes assembling can provide more than 80 motifs of scaffold (Markush structures).

The triazole ring formed by click chemistry is a good bioisostere in drug discovery. Norrild et al. also applied the click chemistry for Hsp90 inhibitors and obtained a more potent lead compared to NVP-AUY992.[35] At the same time, the triazole ring also matches the chemotypes C1, C2, C4, and C7. All of these encourage us to perform click chemistry for chemotypes assembling. According to the chemotypes and click chemistry, several virtual leads were formed and synthesized. A series *in vitro* studies were then applied, **3d** and **3n** were selected due to their potent Hsp90 binding affinity and inhibition effects. Compound **3d** exhibited selectivity on nasopharyngeal carcinoma against liver cancer and cervical carcinoma compared to **3n** and 17-AAG. A possible reason is the isoform selectivity of **3d** (Table S2).[36] Compound **3d** exhibited around 10-fold activity on Hsp90α, Hsp90β, and TRAP1 over GRP94, while 17-AAG showed potent activity on GRP94. Compound **3d** was further optimized due to its selectivity on nasopharyngeal carcinoma. Compound **4f** with the most potent activity (IC_{50} of 160 nM on Hsp90 and 40 nM on nasopharyngeal carcinoma) was obtained. Unusually, the cell apoptosis effect is stronger than the ATPase inhibition effect. Hsp90 is a central chaperone that directs the folding and conformational maturation of its clients. The inhibition of Hsp90 will cause several proteins disfunction or degradation like AKT and HER2. This will lead a multipathway disturbed and therefore cause more potent inhibition effects on cell death.

https://dx.doi.org/10.1021/acs.jmedchem.0c01521
J. Med. Chem. 2021, 64, 2010−2023

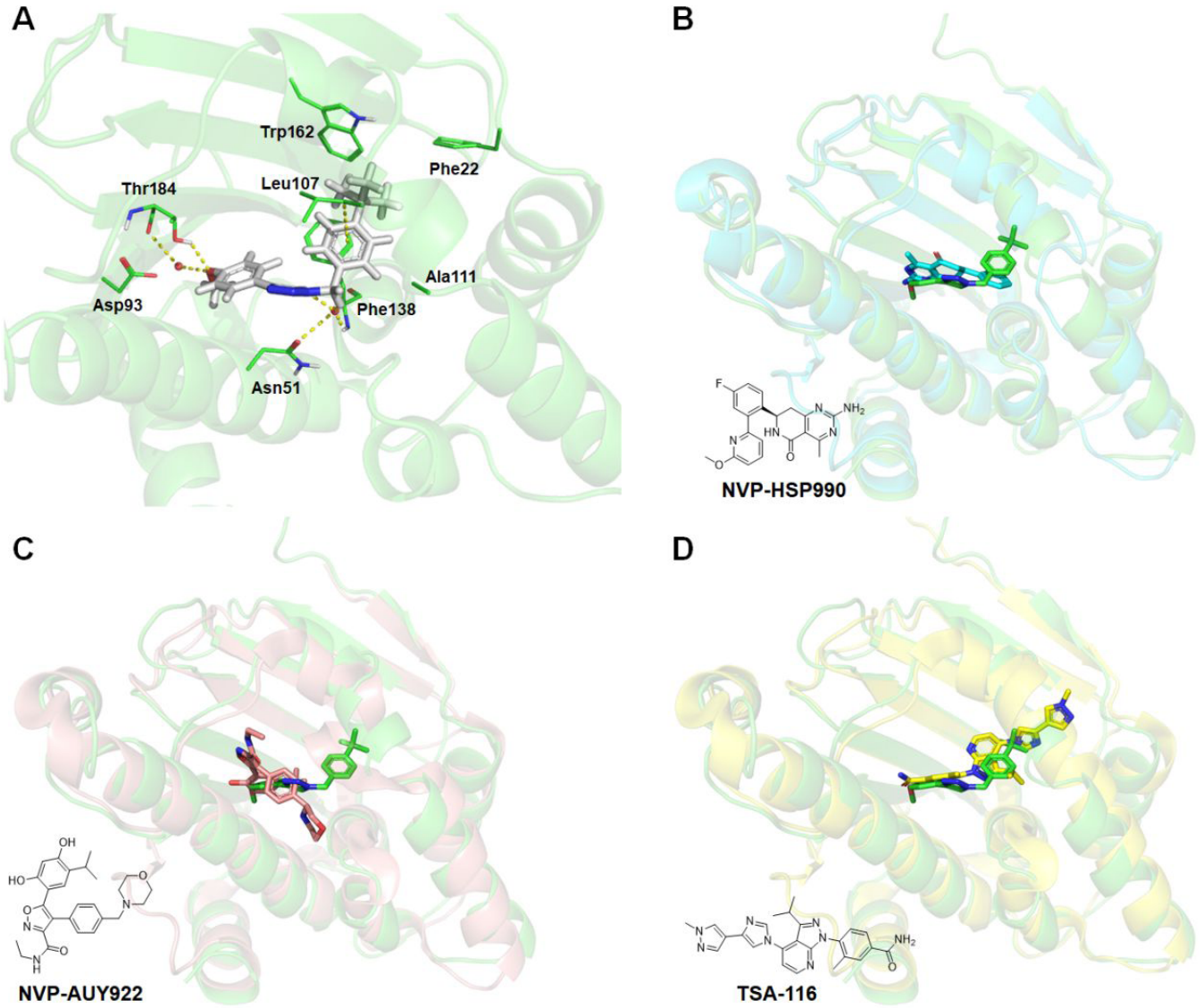

Figure 3. (A) Binding model of compound **3d** with Hsp90α (PDB ID: 4W7T). Compound **3d** binds to Thr184 through a water bridge (red ball). (B) Overlay of compound **3d** with NVP-HSP990 (blue color, PDB ID: 4W7T). (C) Overlay of compound **3d** with NVP-AUY922 (red color, PDB ID: 2VCI). (D) Overlay of compound **3d** with TSA-116 (yellow color, PDB ID: 5ZR3).

CONCLUSIONS

In summary, with chemotyping analysis approach and click chemistry, we have designed, synthesized, and validated new Hsp90 inhibitors with a novel scaffold. *In vitro* and *in vivo* experiments demonstrate that the new inhibitor can be a promising lead for nasopharyngeal carcinoma treatment. Our method might be applied in discovering new ligands against the targets that structures of the binding models are not well understood. Of cause, it will be even better if the binding mechanisms are understood.

EXPERIMENTAL SECTION

Materials. Chemicals were purchased from Energy Chemical Co., Sigma-Aldrich Co., or Tokyo Chemical Industry Co. and utilized without further purification. Solvents were distilled prior to use. For *in vitro* and *in vivo* assay, RPMI 1640 medium and Lipofectamine 2000 were purchased from Thermo Fisher (Thermo Fisher Scientific); Dulbecco's modified Eagle's medium (DMEM) and fetal bovine serum (FBS) were purchased from Gibco (Gibco); penicillin and streptomycin were purchased from Hyclone (Hyclone); and phosphate-buffered saline (PBS) was purchased from Gibco (Gibco, NY). Cell apoptosis was detected using Annexin V-FITC Apoptosis Detection Kit (Yeasen, China). ATPase activity was detected using the ATP, nicotinamide adenine dinucleotide (NADH), phosphoenolpyruvate (PEP), and pyruvate kinase/lactic dehydrogenasea. 3-(4,5-Dimethyl-2-thiazolyl)-2,5-diphenyl-2*H*-tetrazolium bromide (MTT) and cell dissociation solution were obtained from Sigma-Aldrich (Sigma-Aldrich, St Louis, MO).

NMR Spectroscopy and Mass Spectrometry. ^{1}H NMR and ^{13}C NMR spectra were collected on a BRUKER 400 MHz spectrometer and were calibrated with tetramethylsilane. The NMR data are displayed as follows: chemical shifts (δ) are recorded as ppm, coupling constants (J) in hertz (Hz), integrity as the number of protons, and multiplicity as s (singlet), d (doublet), t (triplet), q (quartet), quintet, sextet, and m (multiplet). Mass spectra were obtained on a Shimadzu LCMS-2010EV utilizing the electron-spray ionization method (ESI-MS). Thin-layer chromatography (TLC) was carried out using plates coated with silica gel GF254, purchased from Merck. Column chromatography was performed using Merck silica gel 60 (70−230 mesh).

Purity. Purity of all final compounds was ≥95%, as determined by high-performance liquid chromatography (HPLC, SHIMADZU LC-

https://dx.doi.org/10.1021/acs.jmedchem.0c01521
J. Med. Chem. 2021, 64, 2010−2023

Table 4. Compounds 4a−f and 5a,b with Their Binding Affinities on Hsp90 Homologues and Inhibition Effects on CNE2 Cells

Compds	Structures	Hsp90α IC_{50} (μM)	Hsp90β IC_{50} (μM)	CNE2 IC_{50} (μM)
4a	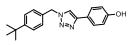	1.3 ± 0.8	1.8 ± 0.2	5.6 ± 1.3
4b	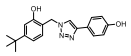	>40	>40	>20
4c	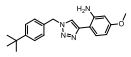	>40	>40	>20
4d	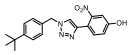	1.7 ± 0.3	1.7 ± 0.5	1.6 ± 0.3
4e	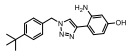	13.7 ± 1.0	14.6 ± 0.2	1.6 ± 0.2
4f	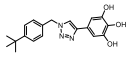	0.16 ± 0.02	0.18 ± 0.06	0.04 ± 0.001
5a	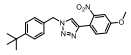	5.0 ± 3.8	5.0 ± 2.7	1.6 ± 0.5
5b	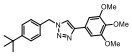	2.7 ± 4.2	2.7 ± 4.0	1.8 ± 0.1
17-AAG		0.85 ± 0.25	0.81 ± 0.13	3.03 ± 0.57

20AT, Japan). Compounds were dissolved at a concentration of 0.5 mg/mL in methanol. Then, 150 μL of the sample was injected into an Agilent XDB-C18 HPLC column (4.6 m × 250 mm; particle size, 5 μm) and chromatographed using a gradient of water/MeCN from 90:10 to 50:50 for 15 min at a flow rate of 250 μL/min. UV absorption was detected from 100 to 950 nm using a diode array detector.

Animals. We performed all procedures on mice and rats with approval by the Sun Yat-sen University Institutional Animal Care and Use Committee. The C57BL/6 mice and female Sprague-Dawley (SD) rats were obtained from Guangdong Medical Lab Animal Center. The mice and rats were maintained in pressurized ventilated cages under conditions of repeated controlled illumination (12 h dark; 12 h light) with ad libitum access to sterilized water and food.

General Synthesis Procedure. Bromide-substituted compound **1**, NaN_3, and CuI were added into dimethyl sulfoxide (DMSO) and H_2O (5:1). The mixture was stirred at room temperature for 0.5 h. Then, the alkene-substituted materials **2** and DBU were added into the mixture and stirred at 70 °C for 8 h. The mixture was followed by extraction with EtOAc. The extract was then washed with water brine, dried over Na_2SO_4, and evaporated *in vacuo*. The residue was purified by column chromatography to give products as a solid.

*6-(4-(4-Methoxyphenyl)-1H-1,2,3-triazol-1-yl)isoquinoline (**3a**).* The general procedure was applied with 6-bromoisoquinoline (208 mg, 1 mmol), NaN_3 (65 mg, 1 mmol), CuI (19 mg, 0.1 mmol), 4-*t*-butylphenylacetylene (158 mg, 1 mmol), and DBU (304 mg, 2 mmol) to provide product **3a** as a white solid (259 mg, 79%). ^{1}H NMR (400 MHz, $CDCl_3$) δ 8.91 (s, 1H), 8.20 (d, J = 8.0 Hz, 1H), 8.07 (s, 1H), 7.89 (d, J = 8.0 Hz, 1H), 7.71 (d, J = 8.0 Hz, 2H), 7.62 (s, 1H), 7.43 (d, J = 8.0 Hz, 1H), 7.39 (d, J = 8.0 Hz, 1H), 7.38 (d, J = 8.0 Hz, 2H), 1.35 (s, 9H). ^{13}C NMR (100 MHz, $CDCl_3$) δ 152.5, 151.3, 148.0, 143.4, 136.6, 131.4, 130.2, 128.9, 128.0, 127.4, 127.3, 125.5, 125.4, 123.9, 120.9, 34.2, 31.3. ESI-MS m/z: 329.16 $[M + H]^+$.

*6-(4-(4-(tert-Butyl)phenyl)-1H-1,2,3-triazol-1-yl)isoquinoline (**3b**).* The general procedure was applied with 6-bromoisoquinoline (208 mg, 1 mmol), NaN_3 (65 mg, 1 mmol), CuI (19 mg, 0.1 mmol), 1-ethynyl-4-methoxybenzene (132 mg, 1 mmol), and DBU (304 mg, 2 mmol) to provide product **3b** as a white solid (163 mg, 54%). ^{1}H NMR (400 MHz, $CDCl_3$) δ 8.98 (s, 1H), 8.25 (d, J = 8.0 Hz, 1H), 7.98 (d, J = 8.0 Hz, 1H), 7.66 (s, 1H), 7.55 (s, 1H), 7.55 (d, J = 8.0 Hz, 2H), 7.42−7.40 (m, 2H), 7.05 (d, J = 8.0 Hz, 2H), 3.83 (s, 3H). ^{13}C NMR (100 MHz, $CDCl_3$) δ 160.6, 152.5, 148.0, 143.4, 136.6, 131.4, 130.2, 128.9, 127.4, 123.9, 122.7, 120.9, 114.8, 55.8. ESI-MS m/z: 302.11 $[M + H]^+$.

*1-(4-(tert-Butyl)benzyl)-4-(4-(tert-butyl)phenyl)-1H-1,2,3-triazole (**3c**).* The general procedure was applied with 1-bromomethyl-4-(*t*-butyl)benzene (212 mg, 1 mmol), NaN_3 (65 mg, 1 mmol), CuI (19 mg, 0.1 mmol), 4-*t*-butylphenylacetylene (158 mg, 1 mmol), and DBU (304 mg, 2 mmol) to provide product **3c** as a white solid (246 mg, 71%). ^{1}H NMR (400 MHz, $CDCl_3$) δ 7.66 (d, J = 8.0 Hz, 2H), 7.64 (s, 1H), 7.36−7.33 (m, 3H), 7.16 (d, J = 8.0 Hz, 2H), 5.45 (s, 2H), 1.25 (s, 9H), 1.24 (s, 9H). ^{13}C NMR (100 MHz, $CDCl_3$) δ 150.8, 150.2, 147.1, 130.7, 126.8, 126.7, 125.0, 124.7, 124.4, 118.2, 52.9, 33.6, 30.2, 30.2. ESI-MS m/z: 348.24 $[M + H]^+$.

*1-(4-(tert-Butyl)benzyl)-4-(4-methoxyphenyl)-1H-1,2,3-triazole (**3d**).* The general procedure was applied with 1-bromomethyl-4-(*t*-butyl)benzene (212 mg, 1 mmol), NaN_3 (65 mg, 1 mmol), CuI (19 mg, 0.1 mmol), 1-ethynyl-4-methoxybenzene (132 mg, 1 mmol), and DBU (304 mg, 2 mmol) to provide product **3d** as a white solid (189 mg, 59%). ^{1}H NMR (400 MHz, $CDCl_3$) δ 7.66 (d, J = 8.0 Hz, 2H), 7.50 (s, 1H), 7.32 (d, J = 8.0 Hz, 2H), 7.17 (d, J = 8.0 Hz, 2H), 6.84 (d, J = 8.0 Hz, 2H), 5.44 (s, 2H), 3.74 (s, 3H), 1.21 (s, 9H). ^{13}C NMR (100 MHz, $CDCl_3$) δ 158.5, 150.8, 147.0, 130.7, 126.8, 126.0, 125.0, 122.3, 117.7, 113.1, 113.1, 54.3, 52.9, 33.6, 30.2, 28.7. ESI-MS m/z: 322.18 $[M + H]^+$.

*4-(4-(tert-Butyl)phenyl)-1-(4-phenoxyphenyl)-1H-1,2,3-triazole (**3e**).* The general procedure was applied with 1-bromo-4-phenoxybenzene (248 mg, 1 mmol), NaN_3 (65 mg, 1 mmol), CuI (19 mg, 0.1 mmol), 4-*t*-butylphenylacetylene (158 mg, 1 mmol), and DBU (304 mg, 2 mmol) to provide product **3e** as a white solid (239 mg, 65%). ^{1}H NMR (400 MHz, $CDCl_3$) δ 8.04 (s, 1H), 7.76 (d, J = 8.0 Hz, 2H), 7.66 (d, J = 8.0 Hz, 2H), 7.43−7.41 (m, 2H), 7.34−7.30 (m, 2H), 7.13−7.06(m, 3H), 7.02−6.99 (m, 2H). ^{13}C NMR (100 MHz, $CDCl_3$) δ 156.79, 155.35, 150.55, 147.36, 131.31, 128.99, 126.38, 124.82, 124.56, 123.09, 121.22, 118.37, 118.31, 116.39, 33.70, 30.27. ESI-MS m/z: 370.18 $[M + H]^+$.

*4-(4-Methoxyphenyl)-1-(4-phenoxyphenyl)-1H-1,2,3-triazole (**3f**).* The general procedure was applied with 1-bromo-4-phenoxybenzene (248 mg, 1 mmol), NaN_3 (65 mg, 1 mmol), CuI (19 mg, 0.1 mmol), 1-ethynyl-4-methoxybenzene (132 mg, 1 mmol), and DBU (304 mg, 2 mmol) to provide product **3f** as a white solid (209 mg, 61%). ^{1}H NMR (400 MHz, $CDCl_3$) δ 7.98 (s, 1H), 7.76 (d, J = 8.0 Hz, 2H), 7.66 (d, J = 8.0 Hz, 2H), 7.35−7.31 (m, 2H), 7.13−7.08 (m, 4H), 6.99−6.91 (m, 3H), 3.79 (s, 3H). ^{13}C NMR (100 MHz, $CDCl_{3)}$ δ 158.78, 156.79, 131.31, 128.99, 126.13, 123.10, 121.91, 121.21, 118.39, 118.30, 115.91, 113.31, 54.33. ESI-MS m/z: 344.13 $[M + H]^+$.

*4-(4-(tert-Butyl)phenyl)-1-(2,3-dihydrobenzo[b][1,4]dioxin-6-yl)-1H-1,2,3-triazole (**3g**).* The general procedure was applied with 6-bromo-2,3-dihydrobenzo[*b*][1,4]dioxine (213 mg, 1 mmol), NaN_3 (65 mg, 1 mmol), CuI (19 mg, 0.1 mmol), 4-*t*-butylphenylacetylene (158 mg, 1 mmol), and DBU (304 mg, 2 mmol) to provide product **3g** as a white solid (211 mg, 66%). ^{1}H NMR (400 MHz, $CDCl_3$) δ 8.07 (s, 1H), 7.84 (d, J = 8.0 Hz, 1H), 7.50 (d, J = 8.0 Hz, 2H), 7.34 (s, 1H), 7.26 (d, J = 8.0 Hz, 1H), 4.34 (s, 3H), 1.39 (s, 9H). ^{13}C NMR (100 MHz, $CDCl_3$) δ 151.5, 148.2, 144.1, 144.0, 131.0, 127.5, 125.8, 125.6, 118.0, 117.4, 113.7, 110.2, 64.4, 64.4, 34.7, 31.3. ESI-MS m/z: 336.16 $[M + H]^+$.

*1-(2,3-Dihydrobenzo[b][1,4]dioxin-6-yl)-4-(4-methoxyphenyl)-1H-1,2,3-triazole (**3h**).* The general procedure was applied with 6-bromo-2,3-dihydrobenzo[*b*][1,4]dioxine (213 mg, 1 mmol), NaN_3 (65 mg, 1 mmol), CuI (19 mg, 0.1 mmol), 1-ethynyl-4-methoxybenzene (132 mg, 1 mmol), and DBU (304 mg, 2 mmol) to provide product **3h** as a white solid (127 mg, 51%). ^{1}H NMR (400 MHz, DMSO-d_6) δ 7.78 (s, 1H), 7.27 (s, 1H), 7.18 (d, J = 8.0 Hz,

https://dx.doi.org/10.1021/acs.jmedchem.0c01521
J. Med. Chem. 2021, 64, 2010−2023

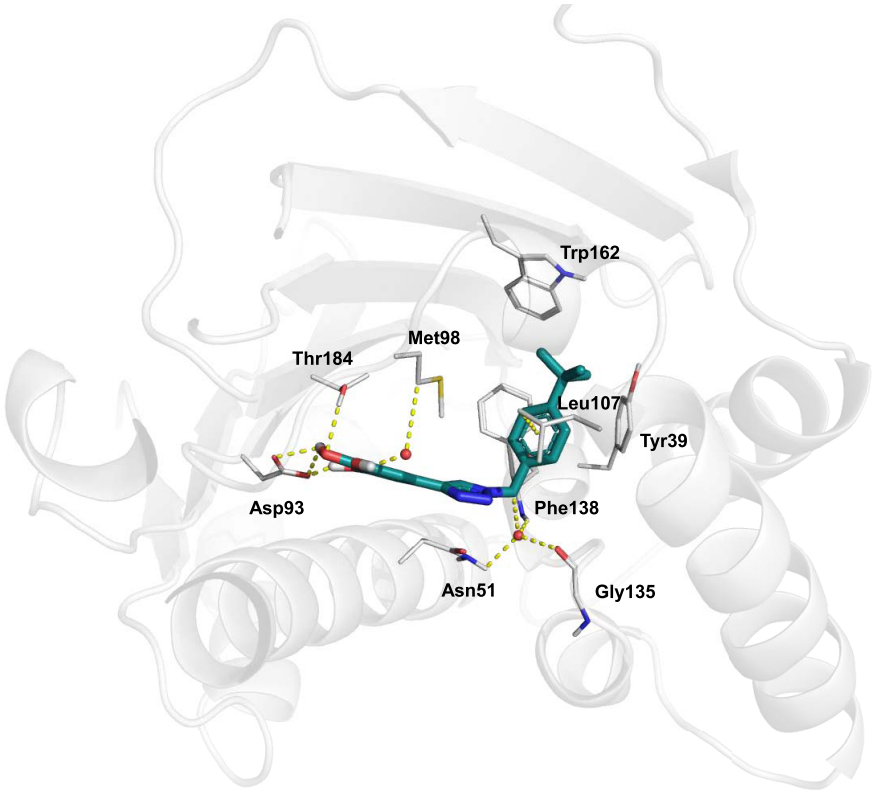

	WT-Hsp90	R93G	L107G	T184G
Binding affinity (μM)	0.063 ± 0.005	103.9 ± 10.9	29.1 ± 4.1	81.4 ± 5.5

Figure 4. Binding model of compound **4f** with Hsp90α (PDB ID: 4W7T) and binding affinity of **4f** with WT-Hsp90α or mutated Hsp90α. The H-bonds are represented as yellow dashed lines. Waters are represented as the red ball.

2H), 6.95 (s, 1H), 6.89−6.77 (m, 3H), 4.30−4.29 (m, 4H), 3.82 (s, 3H). ^{13}C NMR (100 MHz, DMSO-d_6) δ 159.7, 147.5, 144.3, 144.0, 130.9, 127.1, 123.4, 119.1, 118.4, 114.9, 113.4, 109.6, 64.8, 64.6, 55.7. ESI-MS m/z: 310.11 [M + H] $^+$.

*1-(Benzo[d][1,3]dioxol-5-yl)-4-(4-(tert-butyl)phenyl)-1H-1,2,3-triazole (**3i**).* The general procedure was applied with 5-bromobenzo-[d][1,3]dioxole (200 mg, 1 mmol), NaN_3 (65 mg, 1 mmol), CuI (19 mg, 0.1 mmol), 4-t-butylphenylacetylene (158 mg, 1 mmol), and DBU (304 mg, 2 mmol) to provide product **3i** as a white solid (179 mg, 56%). ^{1}H NMR (400 MHz, $CDCl_3$) δ 7.98 (s, 1H), 7.75 (d, J = 8.0 Hz, 2H), 7.41 (d, J = 8.0 Hz, 2H), 7.24 (d, J = 4.0 Hz, 1H), 7.13 (d, J = 8.0 Hz, 1H), 6.85 (d, J = 8.0 Hz, 1H), 6.01 (s, 2H), 1.29 (s, 9H). ^{13}C NMR (100 MHz, $CDCl_3$) δ 150.5, 147.6, 147.2, 146.9, 130.6, 126.4, 124.8, 124.5, 116.6, 113.1, 107.5, 101.7, 101.1, 33.7, 30.3, 28.7. ESI-MS m/z: 322.14 [M + H] $^+$.

*1-(Benzo[d][1,3]dioxol-5-yl)-4-(4-methoxyphenyl)-1H-1,2,3-triazole (**3j**).* The general procedure was applied with 5-bromobenzo-[d][1,3]dioxole (200 mg, 1 mmol), NaN_3 (65 mg, 1 mmol), CuI (19 mg, 0.1 mmol), 1-ethynyl-4-methoxybenzene (132 mg, 1 mmol), and DBU (304 mg, 2 mmol) to provide product **3j** as a white solid (126 mg, 43%). ^{1}H NMR (400 MHz, DMSO-d_6) δ 8.01 (s, 1H), 7.65 (d, J = 8.0 Hz, 2H), 7.10 (d, J = 8.0 Hz, 2H), 7.08 (d, J = 8.0 Hz, 1H), 6.89 (d, J = 8.0 Hz, 1H), 6.83 (s, 1H), 6.07(s, 2H), 3.84 (s, 3H). ^{13}C NMR (100 MHz, DMSO-d_6) δ 160.6, 148.8, 148.0, 131.4, 128.5, 122.7, 121.8, 118.9, 114.8, 114.6, 109.3, 101.2, 55.8. ESI-MS m/z: 296.09 [M + H] $^+$.

*4-(4-(tert-Butyl)phenyl)-1-(4-(trifluoromethyl)benzyl)-1H-1,2,3-triazole (**3k**).* The general procedure was applied with 1-bromomethyl-4-(trifluoromethyl)benzene (225 mg, 1 mmol), NaN_3 (65 mg, 1 mmol), CuI (19 mg, 0.1 mmol), 4-t-butylphenylacetylene (158 mg, 1 mmol), and DBU (304 mg, 2 mmol) to provide product **3k** as a white solid (183 mg, 51%). ^{1}H NMR (400 MHz, $CDCl_3$) δ 7.67 (d, J = 8.0 Hz, 2H), 7.60 (s, 1H), 7.56 (d, J = 8.0 Hz, 2H), 7.37 (d, J = 8.0 Hz, 2H), 7.34 (d, J = 8.0 Hz, 2H), 5.56 (s, 2H), 1.26 (s, 9H). ^{13}C NMR (100 MHz, $CDCl_3$) δ 150.50, 147.53, 137.75, 127.07, 126.39, 125.10, 125.07, 125.03, 124.76, 124.44, 118.28, 52.46, 33.65, 30.24. ESI-MS m/z: 360.05 [M + H] $^+$.

*4-(4-Methoxyphenyl)-1-(4-(trifluoromethyl)benzyl)-1H-1,2,3-triazole (**3l**).* The general procedure was applied with 1-bromomethyl-4-(trifluoromethyl)benzene (225 mg, 1 mmol), NaN_3 (65 mg, 1 mmol), CuI (19 mg, 0.1 mmol), 1-ethynyl-4-methoxybenzene (132 mg, 1 mmol), and DBU (304 mg, 2 mmol) to provide product **3k** as a white solid (179 mg, 54%). ^{1}H NMR (400 MHz, $CDCl_3$) δ 7.66 (d, J = 8.0 Hz, 2H), 7.58−7.55 (m, 3H), 7.33 (d, J = 8.0 Hz, 2H), 6.87 (d, J = 8.0 Hz, 2H), 5.55 (s, 2H), 3.76 (s, 3H). ^{13}C NMR (100 MHz, $CDCl_3$) δ 158.7, 147.4, 137.7, 133.0, 127.1, 126.0, 125.1, 125.1, 125.0, 121.9, 117.7, 113.2, 113.1, 54.3, 52.5. ESI-MS m/z: 334.10 [M + H] $^+$.

*1-(3,5-Bis(trifluoromethyl)benzyl)-4-(4-(tert-butyl)phenyl)-1H-1,2,3-triazole (**3m**).* The general procedure was applied with 1-(bromomethyl)-3,5-bis(trifluoromethyl)benzene (305 mg, 1 mmol), NaN_3 (65 mg, 1 mmol), CuI (19 mg, 0.1 mmol), 4-t-butylphenylacetylene (158 mg, 1 mmol), and DBU (304 mg, 2 mmol) to provide product **3m** as a white solid (277 mg, 65%). ^{1}H NMR (400 MHz, $CDCl_3$) δ 7.80 (s, 1H), 7.69−7.66 (m, 5H), 7.37 (d, J = 8.0 Hz, 2H), 5.62 (s, 2H), 1.26 (s, 9H). ^{13}C NMR (100 MHz, $CDCl_3$) δ 150.7, 147.8, 136.4, 131.8, 131.4, 126.9, 126.9, 126.2, 124.8, 124.5, 121.8, 121.8, 121.7, 118.3, 51.9, 33.7, 30.22. ESI-MS m/z: 428.14 [M + H] $^+$.

*1-(3,5-Bis(trifluoromethyl)benzyl)-4-(4-methoxyphenyl)-1H-1,2,3-triazole (**3n**).* The general procedure was applied with 1-(bromomethyl)-3,5-bis(trifluoromethyl)benzene (305 mg, 1 mmol), NaN_3 (65 mg, 1 mmol), CuI (19 mg, 0.1 mmol), 1-ethynyl-4-

https://dx.doi.org/10.1021/acs.jmedchem.0c01521
J. Med. Chem. 2021, 64, 2010−2023

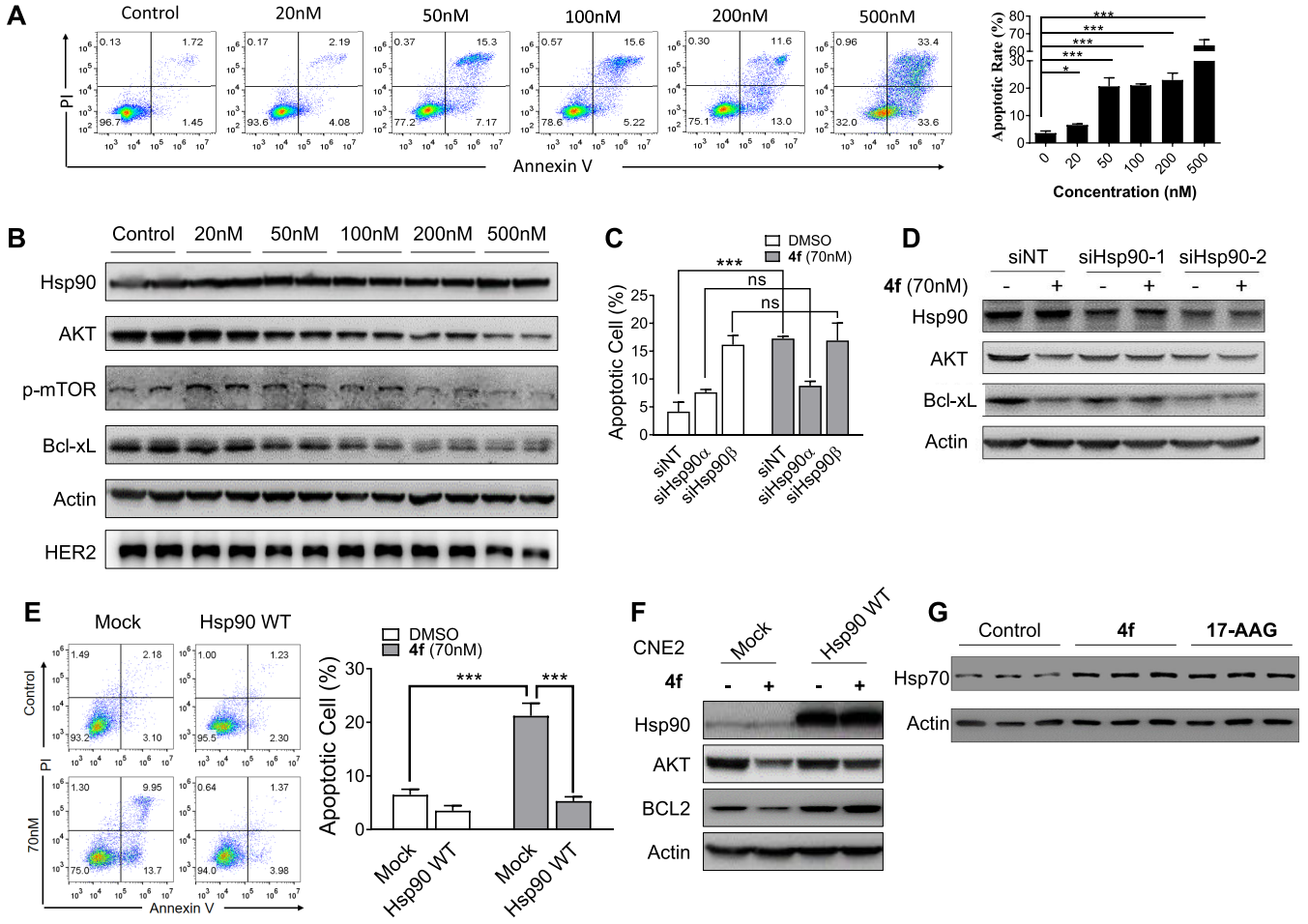

Figure 5. *In vitro* and *in vivo* experiments prove **4f** is a promising lead against nasopharyngeal carcinoma. (A) Quantification of the apoptotic rate in control and different-dose **4f**-treated Annexin V-FITC/PI stained CNE2 cells at 48 h. (B) Western blots analysis of the effects of **4f** on Hsp90, AKT, *p*-mTOR, and Bcl-xL. (C) Changes in cell viability upon Hsp90*α* knockdown with and without compound **4f** at 70 nM. (D) Western blots analysis of the effects of **4f** on Hsp90, AKT, and Bcl-xL when Hsp90 is knockdown. (E) Cell apoptosis of CNE2 in the mock group and the Hsp90 overexpression group without and with **4f** treatment. (F) AKT and BCL-2 expression in the mock group and the Hsp90 overexpression group without and with **4f** treatment. ***: $P \leq 0.001$ compared to related groups; ns: nonsignificant difference compared to related groups.

methoxybenzene (132 mg, 1 mmol), and DBU (304 mg, 2 mmol) to provide product **3n** as a white solid (236 mg, 59%). ^{1}H NMR (400 MHz, $CDCl_3$) δ 7.81 (s, 1H), 7.65 (d, J = 8.0 Hz, 2H), 7.66 (s, 1H), 7.48 (s, 2H), 7.31 (d, J = 8.0 Hz, 2H), 5.50 (s, 2H), 3.84 (s, 3H). ^{13}C NMR (100 MHz, $CDCl_3$) δ 158.7, 147.4, 137.7, 133.0, 127.1, 126.0, 125.1, 125.1, 125.0, 121.9, 117.7, 113.2, 113.1, 54.3, 52.5. ESI-MS m/z: 402.09 $[M + H]^+$.

*6-(4-(Thiophen-2-yl)-1H-1,2,3-triazol-1-yl)isoquinoline (**3o**).* The general procedure was applied with 6-bromoisoquinoline (206 mg, 1 mmol), NaN_3 (65 mg, 1 mmol), CuI (19 mg, 0.1 mmol), 2-ethynylthiophene (108 mg, 1 mmol), and DBU (304 mg, 2 mmol) to provide product **3o** as a yellow solid (239 mg, 86%). ^{1}H NMR (400 MHz, $CDCl_3$) δ 9.15 (s, 1H), 8.56 (d, J = 4.0 Hz, 1H), 7.91−8.86 (m, 3H), 7.39 (t, J = 4.0 Hz, 1H). ^{13}C NMR (100 MHz, $CDCl_3$) δ 151.7, 143.4, 133.9, 132.9, 128.6, 126.7, 126.4, 120.5, 118.3. ESI-MS m/z: 279.16 $[M + H]^+$.

*1-(4-(tert-Butyl)benzyl)-4-(thiophen-2-yl)-1H-1,2,3-triazole (**3p**).* The general procedure was applied with 1-bromomethyl-4-(*t*-butyl)benzene (212 mg, 1 mmol), NaN_3 (65 mg, 1 mmol), CuI (19 mg, 0.1 mmol), 2-ethynylthiophene (108 mg, 1 mmol), and DBU (304 mg, 2 mmol) to provide product **3p** as a white solid (216 mg, 73%). ^{1}H NMR (400 MHz, DMSO-d_6) δ 7.50−7.47 (m, 4H), 7.24−7.22 (m, 3H), 5.48 (s, 2H), 2.21 (s, 9H). ^{13}C NMR (100 MHz, DMSO-d_6) δ 202.6, 175.3, 169.4, 165.6, 158.2, 138.3, 138.1, 114.4, 113.9, 95.70, 91.2, 51.3, 30.7, 21.7. ESI-MS m/z: 298.41 $[M + H]^+$.

*1-(4-Phenoxyphenyl)-4-(thiophen-2-yl)-1H-1,2,3-triazole (**3q**).* The general procedure was applied with 1-bromo-4-phenoxybenzene (248 mg, 1 mmol), NaN_3 (65 mg, 1 mmol), CuI (19 mg, 0.1 mmol), 2-ethynylthiophene (108 mg, 1 mmol), and DBU (304 mg, 2 mmol) to provide product **3q** as a yellow solid (178 mg, 56%). ^{1}H NMR (400 MHz, $CDCl_3$) δ 7.98 (s, 1H), 7.66−7.62 (m, 2H), 7.41−7.40 (m, 1H), 7.35−7.31 (m, 2H), 7.30−7.27 (m, 1H), 7.11−6.99 (m, 6H). ^{13}C NMR (100 MHz, $CDCl_3$) δ 156.9, 129.0, 126.7, 124.4, 123.5, 123.2, 121.3, 118.4, 118.3, 116.2, 28.7. ESI-MS m/z: 320.07 $[M + H]^+$.

*1-(2,3-Dihydrobenzo[b][1,4]dioxin-6-yl)-4-(thiophen-2-yl)-1H-1,2,3-triazole (**3r**).* The general procedure was applied with 6-bromo-2,3-dihydrobenzo[*b*][1,4]dioxine (213 mg, 1 mmol), NaN_3 (65 mg, 1 mmol), CuI (19 mg, 0.1 mmol), 2-ethynylthiophene (108 mg, 1 mmol), and DBU (304 mg, 2 mmol) to provide product **3r** as a white solid (131 mg, 46%). ^{1}H NMR (400 MHz, $CDCl_3$) δ 7.92(s, 0.5H), 8.82 (s, 0.5H), 7.27−7.12 (m, 2H), 7.04−6.90 (m, 3H), 4.24 (s, 2H). ^{13}C NMR (100 MHz, $CDCl_3$) δ 143.1, 131.4, 129.6, 126.7, 124.8, 124.3, 124.1, 123.5, 117.0, 116.3, 112.8, 109.3, 63.4. ESI-MS m/z: 286.05 $[M + H]^+$.

*1-(Benzo[d][1,3]dioxol-5-yl)-4-(thiophen-2-yl)-1H-1,2,3-triazole (**3s**).* The general procedure was applied with 5-bromobenzo[*d*][1,3]-dioxole (200 mg, 1 mmol), NaN_3 (65 mg, 1 mmol), CuI (19 mg, 0.1 mmol), 2-ethynylthiophene (108 mg, 1 mmol), and DBU (304 mg, 2 mmol) to provide product **3s** as a white solid (143 mg, 53%). ^{1}H NMR (400 MHz, DMSO-d_6) δ 9.08 (s, 1H), 7.59 (d, J = 4.0 Hz, 1H),

https://dx.doi.org/10.1021/acs.jmedchem.0c01521
J. Med. Chem. 2021, 64, 2010−2023

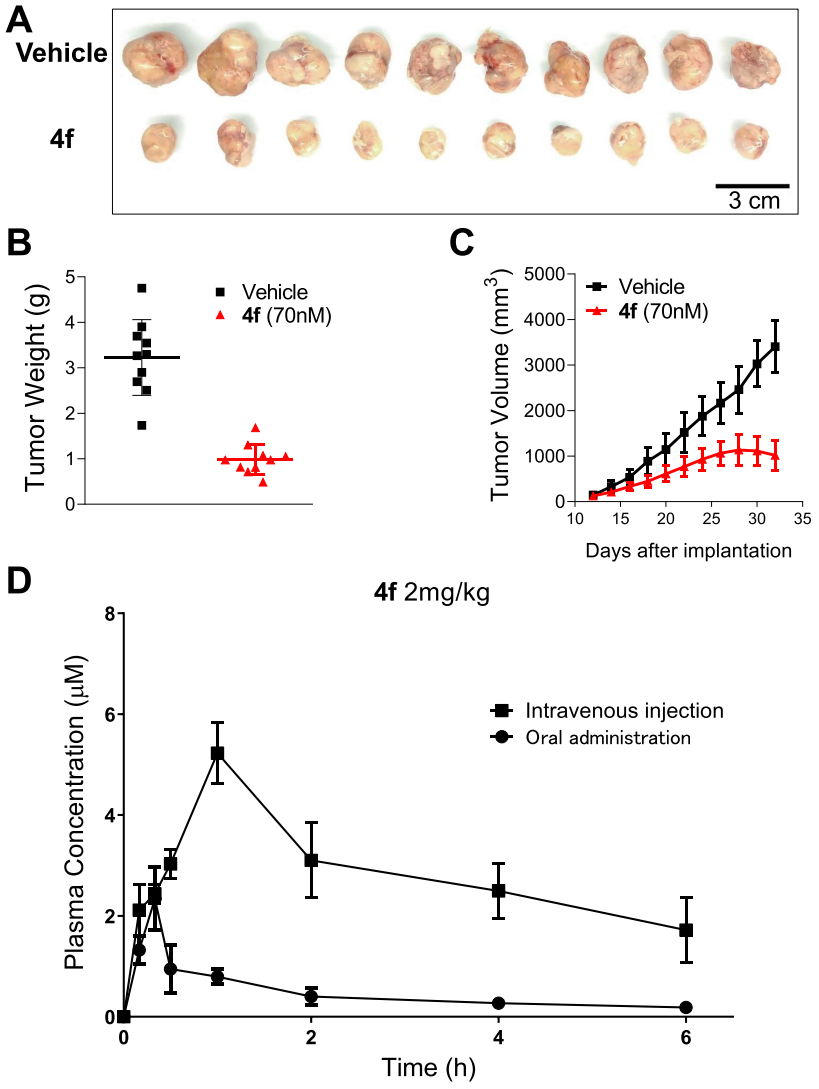

Figure 6. (A) Images of tumors (n = 10) treated with **4f** or vehicle after 32 days. (B) Tumor weight treated with **4f** or vehicle after 32 days. (C) Tumor volume in mice (n = 10) treated for the indicated time with **4f** or vehicle. (D) Pharmacokinetic study of **4f** in mice.

7.53 (d, J = 4.0 Hz, 1H), 7.50 (d, J = 8.0 Hz, 1H), 7.42 (d, J = 8.0 Hz, 1H), 7.19 (t, J = 4.0 Hz, 1H), 7.16 (d, J = 8.0 Hz, 1H). ^{13}C NMR (100 MHz, DMSO-d_6) δ 148.7, 148.0, 142.9, 132.9, 131.4, 128.5, 126.3, 124.9, 119.6, 114.4, 109.1, 102.7, 102.5. ESI-MS m/z: 272.057 [M + H] $^+$.

*4-(Thiophen-2-yl)-1-(4-(trifluoromethyl)benzyl)-1H-1,2,3-triazole (**3t**).* The general procedure was applied with 1-bromomethyl-4-(trifluoromethyl)benzene (225 mg, 1 mmol), NaN_3 (65 mg, 1 mmol), CuI (19 mg, 0.1 mmol), 2-ethynylthiophene (108 mg, 1 mmol), and DBU (304 mg, 2 mmol) to provide product **3t** as a white solid (207 mg, 67%). ^{1}H NMR (400 MHz, $CDCl_3$) δ 7.57 (s, 1H), 7.55 (s, 2H), 7.32 (d, J = 8.0 Hz, 2H), 7.27 (d, J = 4.0 Hz, 1H), 7.21 (d, J = 4.0 Hz, 1H), 7.19 (s, 1H), 6.98 (t, J = 4.0 Hz, 1H), 5.54 (s, 2H). ^{13}C NMR (100 MHz, $CDCl_3$) δ 142.58, 137.45, 131.52, 127.16, 126.62, 125.14, 125.07, 124.24, 123.33, 118.05, 52.53. ESI-MS m/z: 310.05 [M + H] $^+$.

*1-(3,5-Bis(trifluoromethyl)benzyl)-4-(thiophen-2-yl)-1H-1,2,3-triazole (**3u**).* The general procedure was applied with 1-(bromomethyl)-3,5-bis(trifluoromethyl)benzene (305 mg, 1 mmol), NaN_3 (65 mg, 1 mmol), CuI (19 mg, 0.1 mmol), 2-ethynylthiophene (108 mg, 1 mmol), and DBU (304 mg, 2 mmol) to provide product **3u** as a white solid (297 mg, 79%). ^{1}H NMR (400 MHz, $CDCl_3$) δ 7.82 (s, 1H), 7.70 (s, 1H), 7.62 (s, 1H), 7.31 (d, J = 4.0 Hz, 1H), 7.24 (d, J = 4.0 Hz, 1H), 7.00 (t, J = 4.0 Hz, 1H), 5.61 (s, 2H). ^{13}C NMR (100 MHz, $CDCl_3$) δ 142.9, 136.1, 131.9, 131.6, 131.3, 127.1, 126. 7, 124.5, 123.6, 121.9, 120.5, 118.0, 52.0. ESI-MS m/z: 378.04 [M + H] $^+$.

*4-(1-(4-(tert-Butyl)benzyl)-1H-1,2,3-triazol-4-yl)phenol (**4a**).* Compound **3d** (160 mg, 0.5 mmol) was added into hydrobromic acid (48% in water, 10 mL) and stirred at 120 °C for 12 h. Then, the solvent was removed *in vacuo* to give targeted compound **4a** as a white solid (291 mg, 95%). ^{1}H NMR (400 MHz, $CDCl_3$) δ 7.56 (d, J = 8.0 Hz, 2H), 7.51 (s, 1H), 7.33 (d, J = 8.0 Hz, 2H), 7.11 (d, J = 8.0 Hz, 1H), 6.81 (d, J = 8.0 Hz, 1H), 5.45 (s, 2H), 1.24 (s, 9H). ^{13}C NMR (100 MHz, DMSO-d_6) δ 157.7, 151.1, 147.4, 133.7, 128.1, 127.0, 125.9, 122.2, 120.5, 116.1, 53.1, 34.8, 31.5. ESI-MS m/z: 308.39 [M + H]$^+$.

*2-(tert-Butyl)-5-((4-(4-hydroxyphenyl)-1H-1,2,3-triazol-1-yl)-methyl)phenol (**4b**).* The general procedure was applied with 4-(bromomethyl)-1-(*tert*-butyl)-2-methoxybenzene (256 mg, 1 mmol), NaN_3 (65 mg, 1 mmol), CuI (19 mg, 0.1 mmol), 4-*t*-butylphenylacetylene (158 mg, 1 mmol), and DBU (304 mg, 2 mmol) to provide intermediate as a white solid. The intermediate (176 mg, 0.5 mmol) was added into hydrobromic acid (48% in water, 10 mL) and stirred at 120 °C for 12 h. Then, the solvent was removed in vacuum to give targeted compound **4b** as a white solid (141 mg, 88%). ^{1}H NMR (400 MHz, DMSO-d_6) δ 9.57 (s, 1H), 9.44 (s, 1H), 8.39 (s, 1H), 7.65 (d, J = 8.0 Hz, 2H), 7.13 (d, J = 8.0 Hz, 1H), 6.83 (d, J = 8.0 Hz, 2H), 6.72−6.55 (m, 2H), 5.48 (s, 2H), 1.31 (s, 9H). ^{13}C NMR (100 MHz, DMSO-d_6) δ 157.7, 156.5, 147.4, 135.6, 135.2,

https://dx.doi.org/10.1021/acs.jmedchem.0c01521
J. Med. Chem. 2021, 64, 2010−2023

127.1, 127.0, 120.6, 118.4, 116.1, 115.5, 53.0, 34.6, 29.7. ESI-MS *m/z*: 324.38 $[M + H]^+$.

*2-(1-(4-(tert-Butyl)benzyl)-1H-1,2,3-triazol-4-yl)-5-methoxyaniline (**4c**).* The general procedure was applied with 1-bromomethyl-4-(*t*-butyl)benzene (212 mg, 1 mmol), NaN_3 (65 mg, 1 mmol), CuI (19 mg, 0.1 mmol), 1-ethynyl-4-methoxy-2-nitrobenzene (177 mg, 1 mmol), and DBU (304 mg, 2 mmol) to provide intermediate as a white solid. The intermediate (188 mg, 0.5 mmol) was then added into MeOH with Pd/C (50 mg). The air was replaced by H_2. The mixture was stirred at r.t. for 8 h and filtered. The filtrate was collected and purified by falsh column to afford the desired compound **4c** as a white solid (145 mg, 86%). ^{1}H NMR (400 MHz, DMSO-d_6) δ 8.47 (s, 1H), 7.42−7.29 (m, 4H), 6.34−6.18 (m, 3H), 5.59 (s, 2H), 3.35 (s, 3H), 1.26 (s, 9H). ^{13}C NMR (100 MHz, DMSO-d_6) δ 160.2, 151.1, 148.2, 147.6, 133.6, 129.2, 128.2, 126.0, 120.8, 106.6, 103.2, 100.5, 55.2, 53.2, 34.7, 31.5. ESI-MS *m/z*: 337.43 $[M + H]^+$.

*4-(1-(4-(tert-Butyl)benzyl)-1H-1,2,3-triazol-4-yl)-3-nitrophenol (**4d**).* The general procedure was applied with 1-bromomethyl-4-(*t*-butyl)benzene (212 mg, 1 mmol), NaN_3 (65 mg, 1 mmol), CuI (19 mg, 0.1 mmol), 1-ethynyl-4-methoxy-2-nitrobenzene (177 mg, 1 mmol), and DBU (304 mg, 2 mmol) to provide intermediate as a white solid. The intermediate (188 mg, 0.5 mmol) was added into hydrobromic acid (48% in water, 10 mL) and stirred at 120 °C for 12 h. Then, the solvent was removed in vacuum to give targeted compound **4d** as a white solid (169 mg, 96%). ^{1}H NMR (400 MHz, DMSO-d_6) δ 10.82 (brs, 1H), 8.40 (s, 1H), 7.61 (d, *J* = 8.0 Hz, 1H), 7.42 (d, *J* = 8.0 Hz, 2H), 7.28 (d, *J* = 8.0 Hz, 2H), 7.23 (d, *J* = 8.0 Hz, 1H), 7.44−7.11 (m, 1H), 5.60 (s, 2H), 1.27 (s, 9H). ^{13}C NMR (100 MHz, DMSO-d_6) δ 158.4, 149.4, 142.6, 133.5, 132.2, 128.2, 126.0, 123.2, 120.0, 114.8, 110.9, 53.1, 34.8, 31.5. ESI-MS *m/z*: 353.38 $[M + H]^+$.

*3-Amino-4-(1-(4-(tert-butyl)benzyl)-1H-1,2,3-triazol-4-yl)phenol (**4e**).* Compound **4d** (176 mg, 0.5 mmol) was then added into MeOH with Pd/C (50 mg). The air was replaced by H_2. The mixture was stirred at r.t. for 8 h and filtered. The filtrate was collected and purified by flash column to afford desired compound **4e** as a white solid (148 mg, 92%). ^{1}H NMR (400 MHz, DMSO-d_6) δ 8.52 (s, 1H), 7.58 (d, *J* = 8.0 Hz, 1H), 7.41 (d, *J* = 8.0 Hz, 2H), 7.26 (d, *J* = 8.0 Hz, 2H), 6.33 (s, 1H), 6.19 (d, *J* = 8.0 Hz, 1H), 5.58 (s, 2H). ^{13}C NMR (100 MHz, DMSO-d_6) δ 159.4, 148.3, 145.9, 133.1, 130.3, 128.6, 126.1, 123.2, 120.1, 104.7, 101,2, 56.5, 34.7, 31.4. ESI-MS *m/z*: 323.41 $[M + H]^+$.

*5-(1-(4-(tert-Butyl)benzyl)-1H-1,2,3-triazol-4-yl)benzene-1,2,3-triol (**4f**).* The general procedure was applied with 1-bromomethyl-4-(*t*-butyl)benzene (212 mg, 1 mmol), NaN_3 (65 mg, 1 mmol), CuI (19 mg, 0.1 mmol), 5-ethynyl-1,2,3-trimethoxybenzene (192 mg, 1 mmol), and DBU (304 mg, 2 mmol) to provide intermediate as a white solid. The intermediate **5a** (190 mg, 0.5 mmol) was added into hydrobromic acid (48% in water, 10 mL) and stirred at 120 °C for 12 h. Then, the solvent was removed in vacuum to give targeted compound **4f** as a white solid (160 mg, 94%). ^{1}H NMR (400 MHz, DMSO-d_6) δ 8.91 (s, 1H), 8.32 (s, 1H), 8.20 (s, 1H), 7.40 (d, *J* = 8.0 Hz, 2H), 7.28 (d, *J* = 8.0 Hz, 2H), 6.72 (d, *J* = 8.0 Hz, 1H), 5.53 (s, 2H), 1.26 (s, 9H). ^{13}C NMR (100 MHz, DMSO-d_6) δ 151.0, 147.7, 146.8, 133.7, 133.6, 128.2, 125.9, 121.7, 120.6, 104.9, 53.1, 34.7, 31.5. ESI-MS *m/z*: 340.38 $[M + H]^+$. Purity: 97.3%.

Expression and Purification of Proteins. The *Escherichia coli* strain BL21 was transformed with pET28a-Hsp90α, pET28a-Hsp90β, and pET28a-Hsp90α-mutants; cultured in LB medium containing 50 mg/mL kanamycin at 37 °C to an absorbance of 0.6 at 600 nm; and induced with 1 mM IPTG for 16 h at 16 °C before being harvested by centrifugation. The cell pellets were suspended in lysis buffer (10 mM Tris, pH 7.5, 200 mM NaCl, 1 mM DTT) and disrupted by sonication. After centrifugation, the supernatant was applied to a Ni-NTA column and proteins were eluted with elution buffer (10 mM Tris, pH 7.5, 200 mM NaCl, 1 mM DTT, and 400 mM imidazole). The 6-His-tag was removed by digestion with thrombin. The samples were exchanged and further purified with the buffer using size exclusion chromatography (S200 Sephacryl column, GE) in 50 mM HEPES, 200 mM NaCl, and 1 mM DTT. Fractions containing the protein were analyzed using sodium dodecyl sulfate polyacrylamide gel electrophoresis (SDS-PAGE), and fractions showing a single band corresponding to the expected molecular weight were pooled, resulting in >95% pure protein samples.

Surface Plasmon Resonance (SPR) Assay. SPR technology-based binding assays were performed on a Biacore T200 instrument (GE Healthcare) at 25 °C with running buffer PBST (phosphate-buffered saline, pH 7.4, containing 0.005% Tween-20). Protein was dissolved in the coupling buffer (20 μg/mL in 10 mM sodium acetate [pH 5.0]) and immobilized onto the CM5 chip. The chip was first equilibrated with PBST overnight. Inhibitors with 10 μM were serially diluted and injected at a flow rate of 30 μL/min for 120 s (contact phase) followed by 120 s (dissociation phase). The binding data were determined using Biacore T200 evaluation software (GE Healthcare).

ATPase Activity Assay. The ATPase activity assay is based on the conversion of phosphoenolpyruvate (PEP) to pyruvate by pyruvate kinase (PK) coupled to the conversion of pyruvate to lactate by lactate dehydrogenase (LDH) at the expense of NADH.[37] NADH has an excitation wavelength of 340 nm, and the oxidation of NADH to NAD^+ produces a decrease of absorbance at 340 nm. The reaction buffer contained 150 mM Tris-HCl, pH 7.6, 40 mM KCl, 10 mM $MgCl_2$, 1.2 mM ATP, 0.1 mM NADH, 8 mM PEP, and 10 μL of pyruvate kinase/lactic dehydrogenase enzymes (Sigma). The reaction was started by addition of 2 μM Hsp90 protein at 37 °C. The ATPase activity was determined by tracking the decrease in the absorbance at 340 nm. The compounds were added to the reaction mixture to test the inhibition of Hsp90 ATPase activity. 17-AAG as a positive control.

Cells Culture and Cytotoxicity Assay. The poorly differentiated human nasopharyngeal carcinoma (CNE2), HeLa, and HepG2 cell lines were obtained from the Cancer Center of Sun Yat-sen University. CNE2 was cultured in RPMI 1640 medium with 10% fetal bovine serum (v/v) and supplementary 1% (v/v) penicillin/streptomycin. HeLa and HepG2 cell lines were cultured in DMEM with 10% fetal bovine serum (v/v) and supplementary 1% (v/v) penicillin/streptomycin. All cell lines were maintained at 37 °C in a humidified atmosphere with 5% CO_2. Exponentially growing cells were seeded at 3×10^3 cells per well in 96-well culture plates for 24 h. The cells were exposed to increasing concentrations (0−20 μM) of inhibitors for 48 h. The equal volume of DMSO was used as the solvent control. MTT solution (10 μL) was added to each well (0.5 mg/mL) and incubated for another 3 h. Then, the formazan crystals were dissolved in 150 μL of DMSO and light absorbance of the solution was measured at 570 nm, with a reference wavelength of 630 nm, on a multiscanner autoreader (M450; Bio-Rad). The IC_{50} values were calculated using the PrismPad program.

Apoptosis Assay. CNE2 cells were seeded in a 24-well plate (5×10^4 cells/well). After 24 h, the cells were treated with compound (DMSO 0.05%). After 12 h, the cells were washed twice with PBS and collected from the 24-well plate into FACS tubes. The tubes were centrifuged at 1500 rpm for 5 min and washed with 1 mL of PBS. The cells were centrifuged again at 1500 rpm for 5 min and prepared in mastermix (100 μL of 1 × binding buffer, 5 μL of Annexin V/FITC, and 3 μL of PI in each sample). The resuspended cells in 100 μL of mastermix were incubated for 15 min at room temperature in the dark and tested by FACS to evaluate apoptotic cells. Results are represented as mean and s.e.m. of at least three independent experiments.

Immunoblotting. CNE2 (15×10^6 cells/mL) cells were incubated with inhibitors for 24 h. The cells were collected and washed with ice-cold PBS three times. Then, the cells were lysed with RIPA buffer for 30 min on ice. Total cellular protein from each sample was loaded onto 8−12% sodium dodecyl sulfate (SDS) polyacrylamide gel electrophoresis (PAGE) gels. The proteins were transferred to poly(vinylidene fluoride) (PVDF) membranes (Millipore), and the membranes were blocked with 5% nonfat milk for 1 h. The membranes were probed with primary antibodies overnight, washed with TBST for 30 min, exposed to horseradish peroxidase (HRP)-conjugated secondary antibodies for 1 h, and washed again in TBST for 30 min. Immunoreactive material was detected using the chemiluminescence method. Actin was used as the loading control.

https://dx.doi.org/10.1021/acs.jmedchem.0c01521
J. Med. Chem. 2021, 64, 2010−2023

Hsp90α Knockdown Assay. For transient transfection, the cells were transfected with siHsp90-1 (5′-AAAGCGUUCAUGGAAG-CUUUG-3′) or siHsp90-2 (5′-GCUUGACAGAUCCCAGUAATT-3′) at a final concentration of 150 nM using Lipofectamine 2000. The cells were then collected for cytotoxicity assay and immunoblotting assay.

Xenograft Studies. Nude mice (nu/nu, male 6−8 weeks old) were subcutaneously injected with 10×10^6 CNE2 cell on their right flanks. For evaluation of inhibitor using xenograft mice, the molecule was administered daily by i.p. oral with a dose of 1 mg/kg for 6 days after subcutaneous injection of CNE2 cells on the right flank of each mouse. Tumor growth was recorded by measurement of two perpendicular diameters of the tumors over a 3-week period using the formula $4\pi/3 \times (\text{width}/2)^2 \times (\text{length}/2)$. The tumors were harvested and weighed at the experimental endpoint, and the masses of tumors (g) treated with vehicle control (DMSO) and **4f** were compared by a two-tailed unpaired Student's *t* test.

PK Study. Nine male Kunming mice were treated on pharmacokinetic study. All of the animals were 9−11 weeks old with body weight of about 23 g. For two PK studies, four mice per group received a single dose of **4f**. For both intravenous injection and oral administration PK studies, 2 mg/kg of **4f** were given. Blood samples were collected at 0 min, 10 min, 15 min, 30 min, 1 h, 2 h, 4 h, and 6 h post dose. Preparation of samples from the pharmacokinetic studies on the mice was performed using 40 μL of plasma sample, then centrifugation supernatant was obtained. Acetonitrile was added (200 μL) to precipitate plasma proteins, and then the sample was centrifuged for 10 min at 12 000 rpm. The supernatant was transferred to a new tube and frozen at −80 °C until analysis by HPLC (WOOKING, K2025, China). Pharmacokinetic data were analyzed by Pkweb.

Statistics. Mean ± s.d. was calculated to express numerical data and histograms. A two-tailed Student's *t*-test was performed between two groups and a difference was considered statistically significant with $P < 0.05$.

■ ASSOCIATED CONTENT

Supporting Information

The Supporting Information is available free of charge at https://pubs.acs.org/doi/10.1021/acs.jmedchem.0c01521.

NMR spectra and HPLC traces of compound **4f**; SPR response of hit fragments with HSP90 (Figure S1); nontoxicity of compound **4f** on normal human hepatic cells (Figure S2); gray values of AKT expression in CNE2 cells after **4f** treatment (Figure S3); anti-Hsp90 fragments and their frequencies (Table S1); selectivity of 17-AAG, **3d**, and **4f** among Hsp90 isoforms (Table S2); and cytotoxicity of **4a**−**f** on normal cell 293T (Table S3) (PDF)

Molecular Formula Strings (CSV)

■ AUTHOR INFORMATION

Corresponding Authors

Jun Xu − *Research Center for Drug Discovery, School of Pharmaceutical Sciences, Sun Yat-Sen University, Guangzhou 510006, China; School of Biotechnology and Health Sciences, Wuyi University, Jiangmen 529020, China;* orcid.org/0000-0002-1075-0337; Email: junxu@biochemomes.com

Qiong Gu − *Research Center for Drug Discovery, School of Pharmaceutical Sciences, Sun Yat-Sen University, Guangzhou 510006, China;* orcid.org/0000-0001-6011-3697; Email: guqiong@mail.sysu.edu.cn

Daoguang Yan − *Department of Biotechnology, College of Life Science and Technology, Jinan University, Guangzhou 510632, China*; Email: tydg@jnu.edu.cn

Authors

Mengyang Xu − *Research Center for Drug Discovery, School of Pharmaceutical Sciences, Sun Yat-Sen University, Guangzhou 510006, China; Department of Biotechnology, College of Life Science and Technology, Jinan University, Guangzhou 510632, China*

Chao Zhao − *Research Center for Drug Discovery, School of Pharmaceutical Sciences, Sun Yat-Sen University, Guangzhou 510006, China; Shenzhen Cell Inspire Therapeutics Co., Ltd., Shenzhen 518101, China*

Biying Zhu − *Department of Biotechnology, College of Life Science and Technology, Jinan University, Guangzhou 510632, China*

Liangyue Wang − *Research Center for Drug Discovery, School of Pharmaceutical Sciences, Sun Yat-Sen University, Guangzhou 510006, China*

Huihao Zhou − *Research Center for Drug Discovery, School of Pharmaceutical Sciences, Sun Yat-Sen University, Guangzhou 510006, China;* orcid.org/0000-0002-9675-5007

Complete contact information is available at: https://pubs.acs.org/10.1021/acs.jmedchem.0c01521

Author Contributions

M.X. and C.Z. contributed equally to this work. M.X., C.Z., Q.G., and J.X. designed the overall study. C.Z. performed the *in silico* experiments and chemical experiments. M.X. and L.W. performed *in vitro* biological experiments and SPR study. B.Z. performed *in vivo* study. H.Z., D.Y., Q.G., and J.X. supervised the overall study. C.Z., H.Z., D.Y., Q.G., and J.X. wrote and edited the manuscript.

Notes

The authors declare no competing financial interest.

■ ACKNOWLEDGMENTS

This work was funded in part by the National Natural Science Foundation of China (8180131061, 81473138, 81573310, 81803361), National Key R&D Program of China (2017YFB0203403), the Science and Technology Program of Guangzhou (201604020109), the Guangdong Provincial Key Lab. of New Drug Design and Evaluation (Grant 2011A060901014), and the China Postdoctoral Science Foundation(2020M673089).

■ ABBREVIATIONS

FBDD, fragment-based drug design; HER2, receptor tyrosine-protein kinase erbB-2; EGFR, epidermal growth factor receptor; AKT, protein kinase B; BCR-ABL, breakpoint cluster region-c-abl oncogene 1; F2L, fragment to lead; SPR, surface plasmon resonance; NMR, nuclear magnetic resonance; TSA, thermal shift assays; SSSR, smallest set of smallest rings; LXRβ, liver X receptor-β; DSGA, de novo substructure generation algorithm; SCA, scaffold-based classification approach; Hsp90, heat-shock protein 90; SAR, structure−activity relationship; ATP, adenosine triphosphate; PI3K, phosphoinositide 3-kinase; Bcl-xL, B-cell lymphoma-extra large; POC, percent of control

■ REFERENCES

(1) Liu, Z.; Li, H.; He, L.; Xiang, Y.; Tian, C.; Li, C.; Tan, P.; Jing, J.; Tian, Y.; Du, L.; Huang, Y.; Han, L.; Li, M.; Zhou, Y. Discovery of Small-Molecule Inhibitors of the HSP90-Calcineurin-NFAT Pathway against Glioblastoma. *Cell Chem. Biol.* **2019**, *26*, 352−365.

(2) Park, H. K.; Yoon, N. G.; Lee, J. E.; Hu, S.; Yoon, S.; Kim, S. Y.; Hong, J. H.; Nam, D.; Chae, Y. C.; Park, J. B.; Kang, B. H. Unleashing the Full Potential of Hsp90 Inhibitors as Cancer Therapeutics through Simultaneous Inactivation of Hsp90, Grp94, and TRAP1. *Exp. Mol. Med.* **2020**, *52*, 79−91.
(3) Egile, C.; Kenigsberg, M.; Delaisi, C.; Begassat, F.; Do-Vale, V.; Mestadier, J.; Bonche, F.; Benard, T.; Nicolas, J. P.; Valence, S.; Lefranc, C.; Francesconi, E.; Castell, C.; Lefebvre, A. M.; Nemecek, C.; Calvet, L.; Goulaouic, H. The Selective Intravenous Inhibitor of the MET Tyrosine Kinase SAR125844 Inhibits Tumor Growth in MET-Amplified Cancer. *Mol. Cancer Ther.* **2015**, *14*, 384−394.
(4) Kanamaru, C.; Yamada, Y.; Hayashi, S.; Matsushita, T.; Suda, A.; Nagayasu, M.; Kimura, K.; Chiba, S. Retinal Toxicity Induced by Small-Molecule Hsp90 Inhibitors in Beagle Dogs. *J. Toxicol. Sci.* **2014**, *39*, 59−69.
(5) Woodford, M. R.; Dunn, D. M.; Ciciarelli, J. G.; Beebe, K.; Neckers, L.; Mollapour, M. Targeting Hsp90 in Non-Cancerous Maladies. *Curr. Top. Med. Chem.* **2016**, *16*, 2792−2804.
(6) Sun, X.; Barlow, E. A.; Ma, S.; Hagemeier, S. R.; Duellman, S. J.; Burgess, R. R.; Tellam, J.; Khanna, R.; Kenney, S. C. Hsp90 Inhibitors Block outgrowth of EBV-Infected Malignant Cells in vitro and in vivo Through an EBNA1-Dependent Mechanism. *Proc. Natl. Acad. Sci. U.S.A.* **2010**, *107*, 3146−3151.
(7) Shatzer, A.; Ali, M. A.; Chavez, M.; Dowdell, K.; Lee, M. J.; Tomita, Y.; El-Hariry, I.; Trepel, J. B.; Proia, D. A.; Cohen, J. I. Ganetespib, an HSP90 Inhibitor, Kills Epstein-Barr Virus (EBV)-Infected B and T Cells and Reduces the Percentage of EBV-Infected Cells in the Blood. *Leuk. Lymphoma* **2017**, *58*, 923−931.
(8) Srisutthisamphan, K.; Jirakanwisal, K.; Ramphan, S.; Tongluan, N.; Kuadkitkan, A.; Smith, D. R. Hsp90 Interacts with Multiple Dengue Virus 2 Proteins. *Sci. Rep.* **2018**, *8*, No. 4308.
(9) Fuhrmann-Stroissnigg, H.; Ling, Y. Y.; Zhao, J.; McGowan, S. J.; Zhu, Y.; Brooks, R. W.; Grassi, D.; Gregg, S. Q.; Stripay, J. L.; Dorronsoro, A.; Corbo, L.; Tang, P.; Bukata, C.; Ring, N.; Giacca, M.; Li, X.; Tchkonia, T.; Kirkland, J. L.; Niedernhofer, L. J.; Robbins, P. D. Identification of HSP90 Inhibitors as a Novel Class of Senolytics. *Nat. Commun.* **2017**, *8*, No. 422.
(10) Kishinevsky, S.; Wang, T.; Rodina, A.; Chung, S. Y.; Xu, C.; Philip, J.; Taldone, T.; Joshi, S.; Alpaugh, M. L.; Bolaender, A.; Gutbier, S.; Sandhu, D.; Fattahi, F.; Zimmer, B.; Shah, S. K.; Chang, E.; Inda, C.; Koren, J., 3rd; Saurat, N. G.; Leist, M.; Gross, S. S.; Seshan, V. E.; Klein, C.; Tomishima, M. J.; Erdjument-Bromage, H.; Neubert, T. A.; Henrickson, R. C.; Chiosis, G.; Studer, L. HSP90-Incorporating Chaperome Networks as Biosensor for Disease-Related Pathways in Patient-Specific Midbrain Dopamine Neurons. *Nat. Commun.* **2018**, *9*, No. 4345.
(11) Whitesell, L.; Mimnaugh, E. G.; De Costa, B.; Myers, C. E.; Neckers, L. M. Inhibition of Heat Shock Protein HSP90-pp60v-src Heteroprotein Complex Formation by Benzoquinone Ansamycins: Essential Role for Stress Proteins in Oncogenic Transformation. *Proc. Natl. Acad. Sci. U.S.A.* **1994**, *91*, 8324−8328.
(12) Schulte, T. W.; Neckers, L. M. The Benzoquinone Ansamycin 17-Allylamino-17-demethoxygeldanamycin Binds to HSP90 and Shares Important Biologic Activities with Geldanamycin. *Cancer Chemother. Pharmacol.* **1998**, *42*, 273−279.
(13) Kaur, G.; Belotti, D.; Burger, A. M.; Fisher-Nielson, K.; Borsotti, P.; Riccardi, E.; Thillainathan, J.; Hollingshead, M.; Sausville, E. A.; Giavazzi, R. Antiangiogenic Properties of 17-(Dimethylaminoethylamino)-17-demethoxygeldanamycin: an Orally Bioavailable Heat Shock Protein 90 Modulator. *Clin. Cancer Res.* **2004**, *10*, 4813−4821.
(14) Ge, J.; Normant, E.; Porter, J. R.; Ali, J. A.; Dembski, M. S.; Gao, Y.; Georges, A. T.; Grenier, L.; Pak, R. H.; Patterson, J.; Sydor, J. R.; Tibbitts, T. T.; Tong, J. K.; Adams, J.; Palombella, V. J. Design, Synthesis, and Biological Evaluation of Hydroquinone Derivatives of 17-Amino-17-demethoxygeldanamycin as Potent, Water-Soluble Inhibitors of Hsp90. *J. Med. Chem.* **2006**, *49*, 4606−4615.
(15) Brough, P. A.; Aherne, W.; Barril, X.; Borgognoni, J.; Boxall, K.; Cansfield, J. E.; Cheung, K. M.; Collins, I.; Davies, N. G.; Drysdale, M. J.; Dymock, B.; Eccles, S. A.; Finch, H.; Fink, A.; Hayes, A.; Howes, R.; Hubbard, R. E.; James, K.; Jordan, A. M.; Lockie, A.; Martins, V.; Massey, A.; Matthews, T. P.; McDonald, E.; Northfield, C. J.; Pearl, L. H.; Prodromou, C.; Ray, S.; Raynaud, F. I.; Roughley, S. D.; Sharp, S. Y.; Surgenor, A.; Walmsley, D. L.; Webb, P.; Wood, M.; Workman, P.; Wright, L. 4,5-Diarylisoxazole Hsp90 Chaperone Inhibitors: Potential Therapeutic Agents for the Treatment of Cancer. *J. Med. Chem.* **2008**, *51*, 196−218.
(16) Lin, T. Y.; Bear, M.; Du, Z.; Foley, K. P.; Ying, W.; Barsoum, J.; London, C. The Novel HSP90 Inhibitor STA-9090 Exhibits Activity against Kit-Dependent and -Independent Malignant Mast Cell Tumors. *Exp. Hematol.* **2008**, *36*, 1266−1277.
(17) Woodhead, A. J.; Angove, H.; Carr, M. G.; Chessari, G.; Congreve, M.; Coyle, J. E.; Cosme, J.; Graham, B.; Day, P. J.; Downham, R.; Fazal, L.; Feltell, R.; Figueroa, E.; Frederickson, M.; Lewis, J.; McMenamin, R.; Murray, C. W.; O'Brien, M. A.; Parra, L.; Patel, S.; Phillips, T.; Rees, D. C.; Rich, S.; Smith, D. M.; Trewartha, G.; Vinkovic, M.; Williams, B.; Woolford, A. J. Discovery of (2,4-Dihydroxy-5-isopropylphenyl)-[5-(4-methylpiperazin-1-ylmethyl)-1,3-dihydrois Oindol-2-yl]methanone (AT13387), a Novel Inhibitor of the Molecular Chaperone Hsp90 by Fragment Based Drug Design. *J. Med. Chem.* **2010**, *53*, 5956−5969.
(18) Kasibhatla, S. R.; Hong, K.; Biamonte, M. A.; Busch, D. J.; Karjian, P. L.; Sensintaffar, J. L.; Kamal, A.; Lough, R. E.; Brekken, J.; Lundgren, K.; Grecko, R.; Timony, G. A.; Ran, Y.; Mansfield, R.; Fritz, L. C.; Ulm, E.; Burrows, F. J.; Boehm, M. F. Rationally Designed High-affinity 2-Amino-6-halopurine Heat Shock Protein 90 Inhibitors that Exhibit Potent Antitumor Activity. *J. Med. Chem.* **2007**, *50*, 2767−2778.
(19) Saif, M. W.; Takimoto, C.; Mita, M.; Banerji, U.; Lamanna, N.; Castro, J.; O'Brien, S.; Stogard, C.; Von Hoff, D. A phase 1, Dose-escalation, Pharmacokinetic and Pharmacodynamic Study of BIIB021 Administered Orally in Patients with Advanced Solid Tumors. *Clin. Cancer Res.* **2014**, *20*, 445−455.
(20) Bian, Y.; Xie, X. S. Computational Fragment-Based Drug Design: Current Trends, Strategies, and Applications. *AAPS J.* **2018**, *20*, No. 59.
(21) Ayotte, Y.; Bilodeau, F.; Descoteaux, A.; LaPlante, S. R. Fragment-Based Phenotypic Lead Discovery: Cell-Based Assay to Target Leishmaniasis. *ChemMedChem* **2018**, *13*, 1377−1386.
(22) Jencks, W. P. On the Attribution and Additivity of Binding Energies. *Proc. Natl. Acad. Sci. U.S.A.* **1981**, *78*, 4046−4050.
(23) Ascierto, P. A.; McArthur, G. A.; Dreno, B.; Atkinson, V.; Liszkay, G.; Di Giacomo, A. M.; Mandala, M.; Demidov, L.; Stroyakovskiy, D.; Thomas, L.; de la Cruz-Merino, L.; Dutriaux, C.; Garbe, C.; Yan, Y.; Wongchenko, M.; Chang, I.; Hsu, J. J.; Koralek, D. O.; Rooney, I.; Ribas, A.; Larkin, J. Cobimetinib Combined with Vemurafenib in Advanced BRAF(V600)-mutant Melanoma (co-BRIM): Updated Efficacy Results from a Randomised, Double-blind, Phase 3 Trial. *Lancet Oncol.* **2016**, *17*, 1248−1260.
(24) Oltersdorf, T.; Elmore, S. W.; Shoemaker, A. R.; Armstrong, R. C.; Augeri, D. J.; Belli, B. A.; Bruncko, M.; Deckwerth, T. L.; Dinges, J.; Hajduk, P. J.; Joseph, M. K.; Kitada, S.; Korsmeyer, S. J.; Kunzer, A. R.; Letai, A.; Li, C.; Mitten, M. J.; Nettesheim, D. G.; Ng, S.; Nimmer, P. M.; O'Connor, J. M.; Oleksijew, A.; Petros, A. M.; Reed, J. C.; Shen, W.; Tahir, S. K.; Thompson, C. B.; Tomaselli, K. J.; Wang, B.; Wendt, M. D.; Zhang, H.; Fesik, S. W.; Rosenberg, S. H. An Inhibitor of Bcl-2 Family Proteins Induces Regression of Solid Tumours. *Nature* **2005**, *435*, 677−681.
(25) Erlanson, D. A.; Fesik, S. W.; Hubbard, R. E.; Jahnke, W.; Jhoti, H. Twenty Years on: the Impact of Fragments on Drug Discovery. *Nat. Rev. Drug Discovery* **2016**, *15*, 605−619.
(26) Congreve, M.; Carr, R.; Murray, C.; Jhoti, H. A 'Rule of Three' for Fragment-Based Lead Discovery? *Drug Discovery Today* **2003**, *8*, 876−877.
(27) Ertl, P. Cheminformatics Analysis of Organic Substituents: Identification of the Most Common Substituents, Calculation of Substituent Properties, and Automatic Identification of Drug-Like Bioisosteric Groups. *J. Chem. Inf. Comput. Sci.* **2003**, *43*, 374−380.

https://dx.doi.org/10.1021/acs.jmedchem.0c01521
J. Med. Chem. 2021, 64, 2010−2023

(28) Scott, D. E.; Coyne, A. G.; Hudson, S. A.; Abell, C. Fragment-Based Approaches in Drug Discovery and Chemical Biology. *Biochemistry* **2012**, *51*, 4990−5003.
(29) Korczynska, M.; Le, D. D.; Younger, N.; Gregori-Puigjane, E.; Tumber, A.; Krojer, T.; Velupillai, S.; Gileadi, C.; Nowak, R. P.; Iwasa, E.; Pollock, S. B.; Ortiz Torres, I.; Oppermann, U.; Shoichet, B. K.; Fujimori, D. G. Docking and Linking of Fragments To Discover Jumonji Histone Demethylase Inhibitors. *J. Med. Chem.* **2016**, *59*, 1580−1598.
(30) Kozakov, D.; Hall, D. R.; Jehle, S.; Luo, L.; Ochiana, S. O.; Jones, E. V.; Pollastri, M.; Allen, K. N.; Whitty, A.; Vajda, S. Ligand Deconstruction: Why Some Fragment Binding Positions are Conserved and Others are Not. *Proc. Natl. Acad. Sci. U.S.A.* **2015**, *112*, E2585−2594.
(31) Peng, H.; Liu, Z.; Yan, X.; Ren, J.; Xu, J. A De Novo Substructure Generation Algorithm for Identifying the Privileged Chemical Fragments of Liver X Receptorbeta Agonists. *Sci. Rep.* **2017**, *7*, No. 11121.
(32) Zhao, C.; Huang, D.; Li, R.; Xu, Y.; Su, S.; Gu, Q.; Xu, J. Identifying Novel Anti-Osteoporosis Leads with a Chemotype-Assembly Approach. *J. Med. Chem.* **2019**, *62*, 5885−5900.
(33) Tonsing-Carter, E.; Bailey, B. J.; Saadatzadeh, M. R.; Ding, J.; Wang, H.; Sinn, A. L.; Peterman, K. M.; Spragins, T. K.; Silver, J. M.; Sprouse, A. A.; Georgiadis, T. M.; Gunter, T. Z.; Long, E. C.; Minto, R. E.; Marchal, C. C.; Batuello, C. N.; Safa, A. R.; Hanenberg, H.; Territo, P. R.; Sandusky, G. E.; Mayo, L. D.; Eischen, C. M.; Shannon, H. E.; Pollok, K. E. Potentiation of Carboplatin-Mediated DNA Damage by the Mdm2 Modulator Nutlin-3a in a Humanized Orthotopic Breast-to-Lung Metastatic Model. *Mol. Cancer Ther.* **2015**, *14*, 2850−2863.
(34) Voloshin, T.; Alishekevitz, D.; Kaneti, L.; Miller, V.; Isakov, E.; Kaplanov, I.; Voronov, E.; Fremder, E.; Benhar, M.; Machluf, M.; Apte, R. N.; Shaked, Y. Blocking IL1beta Pathway Following Paclitaxel Chemotherapy Slightly Inhibits Primary Tumor Growth but Promotes Spontaneous Metastasis. *Mol. Cancer Ther.* **2015**, *14*, 1385−1394.
(35) Norrild, J. C.; Lauritsen, A.; Björkling, F.; Vadlamudi, S. M. 4-Substituted-6-isopropyl-benzene-1,3-diol Compounds and Their use. WO2009/066060A2, May 28, 2009.
(36) Ohkubo, S.; Kodama, Y.; Muraoka, H.; Hitotsumachi, H.; Yoshimura, C.; Kitade, M.; Hashimoto, A.; Ito, K.; Gomori, A.; Takahashi, K.; Shibata, Y.; Kanoh, A.; Yonekura, K. TAS-116, a Highly Selective Inhibitor of Heat Shock Protein 90 Alpha and Beta, Demonstrates Potent Antitumor Activity and Minimal Ocular Toxicity in Preclinical Models. *Mol. Cancer Ther.* **2015**, *14*, 14−22.
(37) Zhang, T.; Li, Y.; Yu, Y.; Zou, P.; Jiang, Y.; Sun, D. Characterization of Celastrol to Inhibit Hsp90 and dc37 Interaction. *J. Biol. Chem.* **2009**, *284*, 35381−35389.

https://dx.doi.org/10.1021/acs.jmedchem.0c01521
J. Med. Chem. 2021, 64, 2010−2023